

WRDC-TR-89-3089

FREQUENCY DOMAIN DESIGN OF ROBUST CONTROLLERS
FOR SPACE STRUCTURES

ADA 211 172

W.H. Bennett
C. LaVigna

Systems Engineering, Inc. SEI-89-03-15-WB.
7833 Walker Dr., Suite 620
Greenbelt, MD 20770

August 1989

Final Report for Period September 1988 - February 1989

Approved for Public Release; Distribution is Unlimited



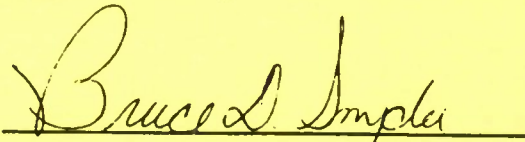
FLIGHT DYNAMICS LABORATORY
WRIGHT RESEARCH AND DEVELOPMENT CENTER .
AIR FORCE SYSTEMS COMMAND
WRIGHT-PATTERSON AIR FORCE BASE, OHIO 45433-6553

NOTICE

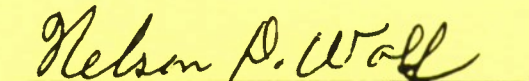
When Government drawings, specifications, or other data are used for any purpose other than in connection with a definitely Government-related procurement, the United States Government incurs no responsibility or any obligation whatsoever. The fact that the government may have formulated or in any way supplied the said drawings, specifications, or other data, is not to be regarded by implication, or otherwise in any manner construed, as licensing the holder, or any other person or corporation; or as conveying any rights or permission to manufacture, use, or sell any patented invention that may in any way be related thereto.

This report is releasable to the National Technical Information Service (NTIS). At NTIS, it will be available to the general public, including foreign nations.

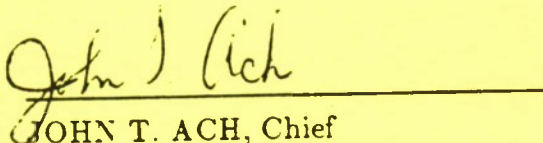
This technical report has been reviewed and is approved for publication.



BRUCE D. SNYDER, CAPT, USAF
Project Engineer
Design & Analysis Methods Group
FOR THE COMMANDER



NELSON D. WOLF, Technical Manager
Design & Analysis Methods Group
Analysis & Optimization Branch



JOHN T. ACH, Chief
Analysis Optimization Branch
Structures Division

If your address has changed, if you wish to be removed from our mailing list, or if the addressee is no longer employed by your organization please notify WRDC/FIBRA, WPAFB, OH 45433-6553 to help us maintain a current mailing list.

Copies of this report should not be returned unless return is required by security considerations, contractual obligations, or notice on a specific document.

UNCLASSIFIED

SECURITY CLASSIFICATION OF THIS PAGE

REPORT DOCUMENTATION PAGE

1a. REPORT SECURITY CLASSIFICATION UNCLASSIFIED			1b. RESTRICTIVE MARKINGS NONE		
2a. SECURITY CLASSIFICATION AUTHORITY			3. DISTRIBUTION/AVAILABILITY OF REPORT Approved for public release; distribution is unlimited.		
2b. DECLASSIFICATION/DOWNGRADING SCHEDULE					
4. PERFORMING ORGANIZATION REPORT NUMBER(S) SEI-89-03-15-WB			5. MONITORING ORGANIZATION REPORT NUMBER(S) WRDC-TR-89-3089		
6a. NAME OF PERFORMING ORGANIZATION Systems Engineering, Inc.		6b. OFFICE SYMBOL (If applicable)	7a. NAME OF MONITORING ORGANIZATION Air Force Wright Research & Development Center (WRDC/FIBRA)		
6c. ADDRESS (City, State and ZIP Code) 7833 Walker Dr. Suite 620 Greenbelt MD 20770			7b. ADDRESS (City, State and ZIP Code) Wright-Patterson Air Force Base, Ohio 45433-6553		
8a. NAME OF FUNDING/SPONSORING ORGANIZATION Strategic Defense Initiative		8b. OFFICE SYMBOL (If applicable)	9. PROCUREMENT INSTRUMENT IDENTIFICATION NUMBER F33615-88-C-3215		
8c. ADDRESS (City, State and ZIP Code) T/IS/SBIR			10. SOURCE OF FUNDING NOS.		
			PROGRAM ELEMENT NO. 63220C	PROJECT NO. 2200	TASK NO. 51
11. TITLE (Include Security Classification) Frequency Domain Design of Robust Controllers for Space Structures					
12. PERSONAL AUTHOR(S) W.H. Bennett and C. LaVigna					
13a. TYPE OF REPORT FINAL		13b. TIME COVERED FROM Sep 88 TO Feb 89		14. DATE OF REPORT (Yr., Mo., Day) 15 89	
15. PAGE COUNT 53					
16. SUPPLEMENTARY NOTATION					
17. COSATI CODES			18. SUBJECT TERMS (Continue on reverse if necessary and identify by block number) SEE ATTACHED		
FIELD	GROUP	SUB. GR.			
19. ABSTRACT (Continue on reverse if necessary and identify by block number) SEE ATTACHED					
20. DISTRIBUTION/AVAILABILITY OF ABSTRACT UNCLASSIFIED/UNLIMITED <input checked="" type="checkbox"/> SAME AS RPT. <input type="checkbox"/> DTIC USERS <input type="checkbox"/>			21. ABSTRACT SECURITY CLASSIFICATION UNCLASSIFIED		
22a. NAME OF RESPONSIBLE INDIVIDUAL Dr. V. Venkayya			22b. TELEPHONE NUMBER (Include Area Code) (513)255-7191		22c. OFFICE SYMBOL WRDC/FIBRA

Small Business Innovation Research (SBIR) Program

Phase 1 - Summary Report

Contract No. F33615-88-C-3215

Topic No.: SDI87-12

Small Business Firm: SYSTEMS ENGINEERING, INC.¹

Principal Investigator: Dr. William H. Bennett

Proposal Title: Frequency Domain Design of Robust Controllers for Space Structures

Project Summary:

The purpose of the Phase 1 effort was to investigate and demonstrate the feasibility of a new class of computational algorithms for the design of high performance control laws for flexible space structures based on frequency response modeling and to consider advanced techniques for the implementation of real time control for precision (wide bandwidth) applications. Typical applications requiring advanced realtime control of flexible space structure include vibration suppression and isolation of payload subsystems. Performance of vibration suppression and isolation systems are critical factors effecting achievable levels of performance for space based optical systems.

In the Phase 1 effort, a prototype software code was developed for testing computational algorithms for spectral factorization, causal projection, and coprime factorization—critical steps in frequency domain design of precision control laws. Several representative models of vibration suppression and isolation of flexible structures were developed and control laws were designed and tested. The innovative approach for frequency domain computations employed is based on sampling and interpolation of the system frequency response. Results from Phase 1 study clearly demonstrate the efficiency and

¹A Division of Techno-Sciences, Inc.

numerical stability of the computational algorithms for both irrational (distributed parameter) transfer function models and various rational (lumped parameter) approximate models of structural elasticity. The feasibility of innovative realtime control implementations based on state-of-the-art VLSI technology and modern digital signal processing was considered in the Phase 1 effort. Design and testing of such controller implementations will form the basis of the Phase 2 proposal.

Anticipated Benefits/Applications:

The project has demonstrated a radical and innovative approach to realtime control for flexible space structures which has the potential to handle large degree-of-freedom motions by a computationally efficient approach. The demonstration of realtime control by FIR based digital processing will provide a new and effective approach for realtime control implementation applicable to a wide variety of space-based payload systems with requirements for precision stabilization, pointing, and vibration isolation. Frequency response modeling is potentially important for a wide variety of applications where active control of elastic mechanical vibration are the primary performance criterion effecting system accuracy and precision. Such systems include various space based optical and rf sensors systems as well as directed energy weapon platforms with precision pointing requirements.

Key Words:

flexible structures, digital control, FIR filters, distributed parameter control theory

CONTENTS

Contents

1	Phase 1 Project Objectives and Progress Summary	1
2	Technical Background for Project Innovation	3
2.1	Transfer Function Models for Flexible Structures	3
2.1.1	Frequency Response Models for Elastic Structures	6
2.2	Control Synthesis via Wiener-Hopf Methods	9
2.3	Wiener-Hopf Design for A Class of Irrational Transfer Functions	13
3	Phase 1 Project Results: Computation of optimal control for flexible structures by frequency sampling.	15
3.1	Frequency Response Design Method for Vibration Control	15
3.2	Computational Algorithms for Frequency Domain Control Design	16
3.2.1	Coprime (stable) Factorization	16
3.2.2	Solution of Diophantine Relations	18
3.2.3	Spectral Factorization and Causal Projection	18
3.3	Development and testing the interactive software environment	26
3.3.1	Objectives of the prototype software environment	26
3.3.2	Testing and Benchmarks	28
3.3.3	Considerations for later versions	30
3.4	Benchmark Problems Considered in Phase 1	32
3.4.1	Control of a pinned-pinned beam.	32
3.4.2	Vibration Isolation for a Simple Elastic Structure.	35
3.5	Realtime Control Law Implementation	45
4	Conclusions and Directions	50

List of Figures

1.1	The realization/implementation paradigm of modern control theory.	2
2.1	Multiloop Control Configuration for Wiener-Hopf Design	10
3.1	An example of the start-up menu.	26
3.2	Residual computation summary from MIMO case benchmark problem.	27
3.3	An example of a saturation cost vs. tracking cost plot.	28
3.4	The plotting menu.	29
3.5	The plot type menu.	29
3.6	Controller frequency response with 1024 points.	31
3.7	Controller frequency response with 256 points.	31
3.8	Pinned-Pinned Beam Control Problem.	32
3.9	Frequency response for pinned-pinned beam control.	34
3.10	PSD for disturbance and sensor noise inputs for beam control.	34
3.11	Convergence of filter spectral factorization for pinned-pinned beam.	36
3.12	Spectral Factors for pinned-pinned beam control.	36

LIST OF TABLES

3.13 Tracking vs. Saturation Tradeoff for Beam Control.	37
3.14 Frequency response for pinned-pinned beam control.	37
3.15 Tracking vs. Saturation Tradeoff for Beam Control.	38
3.16 Design Tradeoff using Sensitivity Function for Beam Control.	38
3.17 Nyquist Plot of Beam Control Loop for $k = .1$	39
3.18 Optimal Controller Frequency Response for $k = .1$	39
3.19 Vibration Isolation Model with Flexible Structure.	43
3.20 Pole/Zero plot for Vibration Isolation Model.	43
3.21 Pole/zero Locations for the Coprime Factors.	44
3.22 Singular Value plots of the Sensitivity Function for $k = .5$	46
3.23 Bode plots for the scalar elements of $C(s)$	47
3.24 Singular value plots of $P(s)$	48
3.25 Option for Stable FIR controller implementation	50

List of Tables

3.1 Properties of Matrix Data Sequences	25
3.2 Benchmark computational times and storage requirements.	30
3.3 Model Parameters for Vibration Isolation Problem.	40

1 Phase 1 Project Objectives and Progress Summary

Available methods for design of complex, multiloop control systems for flexible structures are currently quite limited. Current methods are largely based on state space models obtained by modal truncation and controllers are designed by LQG optimization [1]. Achieving *precision control* will depend on the ability to optimally assess design tradeoffs for models which capture the essential *distributed parameter* nature of the dynamic phenomenon involved [2].

The Modern Control Theory Paradigm: Computation and Implementation by State Space Methods Modern methods in control system design are based on a class of mathematical models for the linear (small amplitude) response of systems (called *state space models*) resulting from modeling the system response as a system on first order Ordinary Differential Equations (ODE's) in time. Optimization of the system time responses is used to resolve certain basic engineering tradeoffs. State space models are particularly significant for time response optimization since they provide an *internal realization* of the system dynamics in terms of a system *state* which codifies the past history of the system response up to the current time. The concept of a state space realization has proven advantageous (at least for low-order systems) for several reasons including the fact the computational algorithms for time response optimization can be described in terms of constant real matrices. Such computational algorithms can be readily supported by reliable numerical software running on a standard digital computer.

In the theory the system response is modeled by a state space model;

$$\begin{aligned}\dot{x}(t) &= Ax(t) + Bu(t), \\ y(t) &= Cx(t),\end{aligned}$$

where $x(t) \in \mathbb{R}^n$ is the system state, $y(t) \in \mathbb{R}^p$ is the vector of system outputs, and $u(t) \in \mathbb{R}^m$ is the vector of system inputs. Control system design methods are based on the *separation* of state variable feedback and asymptotic state estimator (observer) designs. The resulting control compensator suggested by this process of separate design steps can be realized as shown in Figure 1.1. Here the triangular blocks designate an integration operation for continuous time system realizations as described above. The picture (drawn in this way) is suggestive of the principal technology for simulation of dynamical systems—popular in the 1950-1970's—associated with analog or hybrid computers.

As the performance of digital computers increased while their size and power requirements decreased a range of applications for realtime control using digital computers became possible. The modern control paradigm was then extended by considering the state space realization for the equivalent sampled-data system of the form

$$\begin{aligned}x((k+1)T) &= Ax(kT) + Bu(kT), \\ y(kT) &= Cx(kT),\end{aligned}$$

where T is the (uniform) sampling interval. In this case the implementation/realization paradigm carries over directly by considering the triangular blocks in Fig. 1.1 to be a unit

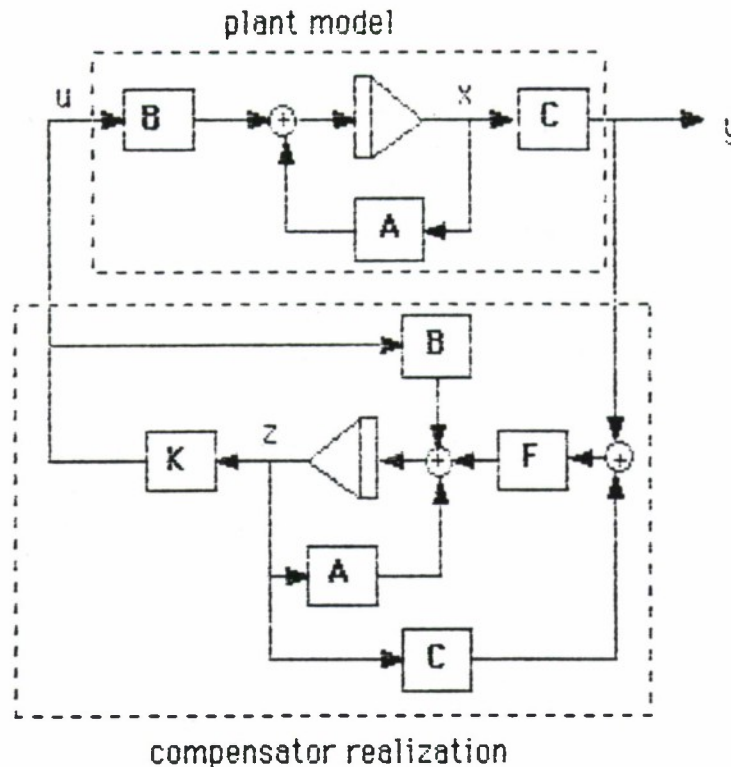


Figure 1.1: The realization/implementation paradigm of modern control theory.

delay of time T . However, it is apparent that such a component based approach to implementation offers a constrained view of options for realtime control implementation in a digital computer.

It is the basic proposition of this project (and the phase 2 proposal will focus on this issue) that the above component based approach to control law implementation by state space realization is essentially obsolete given the state-of-the-art in high speed VLSI designed for signal processing (i.e. real-time applications.) We contend that the various technologies for high speed and very wide time-bandwidth product computations (including advanced VLSI and special acousto-optical systems) are now mature enough to investigate alternate paradigms for realtime control law implementation.

State Space Alternatives for Distributed Parameter Systems. For application to control design computations for flexible space structures we note the use of state space models may be particularly awkward for the typical computations required to obtain time responses. This is true in general for distributed parameter systems since the appropriate state space models will involve a coupled set of integral-partial differential equations (IPDE's). However, for the class of models typically encountered in dynamics of space structures we observe that transfer function (or frequency response) models may be particularly significant.

We suggest that the use of transfer function models for control design can offer significant alternatives for control system design for the following reasons.

1. The interplay between 'state-space' and 'input-output' methods—evident in the theory

of finite-dimensional systems [3, 4]—is even more important for distributed parameter systems with potential for profound results in basic engineering methods.

2. Precise engineering specifications for distributed control system designs are extremely difficult to formulate in terms of state-space models (e.g., in terms of PDE's and their coefficients). These specifications can be rather easily characterized in terms of the system frequency response.
3. By working with the transfer function model directly, alternate control law implementations can be discovered which may be simple to implement and very effective.
4. It is convenient to characterize model uncertainty in a frequency domain setting and this approach provides insight useful for control system design [5].

Remarks on Implementation of Distributed Control For a variety of reasons distributed state feedback control laws may be difficult to implement and state observer-based control will require the on-line realization of a distributed parameter system. In the modern, state-space approach to design the control law realization is linked with the state space model for the system. We assert that this paradigm may seriously restrict design options for control law realization for a large class of linear, time-invariant systems including distributed parameter effects. We prefer to think more generally of a linear, dynamic control law as modeled by a convolution equation,

$$u(t) = C(t) * y(t),$$

where $y(t)$ are available sensor measurements and $u(t)$ are control actuation signals. For linear, time-invariant system models the control law can be *specified* by its impulse response $C(t)$ or in the frequency domain as a transfer function $\hat{C}(s)$ which may be irrational. The principal innovation of this project is that control system design for distributed parameter systems may benefit from decoupling the computation and realization design steps. A principal project objective of this study is to assess the capability for alternate methods for control law realization which may offer reasonable approximation of an optimal irrational transfer function for a control law.

2 Technical Background for Project Innovation

2.1 Transfer Function Models for Flexible Structures

Generic models for the elastic response of flexible structures are often described as spatial continuum via a Partial Differential Equation (PDE) of the form,

$$m(z) \frac{\partial^2 w(t, z)}{\partial t^2} + D_0 \frac{\partial w(t, z)}{\partial t} + A_0 w(t, z) = F(t, z) \quad (2.1)$$

where $w(t, z)$ is an N-vector of displacements of a structure Ω with respect to some equilibrium for Ω is a bounded, open set in \mathbb{R}^N [1]. The (vector) $z \in \Omega$ is a coordinate in Ω .

We assume the boundary $\partial\Omega$ is smooth. The mass density $m(z)$ is positive definite and bounded on $\partial\Omega$. The damping term $D_0\partial w/\partial t$ models both (asymmetric) gyroscopic and (symmetric) structural damping effects. The internal restoring force A_0w is generated by a time-invariant, differential operator A_0 for the structure. For most common structural models, A_0 is an unbounded, differential operator with domain $D(A_0)$ consisting of certain smooth functions satisfying appropriate boundary conditions on $\partial\Omega$. Thus, for these problems, $D(A_0)$ is typically dense in the Hilbert space $\mathcal{H}_0 = \mathcal{L}_2(\Omega)$ endowed with its natural inner product $\langle x, y \rangle_0 = \int_{\Omega} x^T(z)y(z) dz$. Often (but not always), the spectrum of A_0 , $\sigma(A_0)$, consists of discrete eigenvalues with associated eigenfunctions which constitute a basis for $\mathcal{L}_2(\Omega)$.

The applied force distribution $F(t, z)$ can be thought of as consisting of three components

$$F(t, z) = F_d(t, z) + F_c(t, z) + F_a(t, z) \quad (2.2)$$

where F_d is N-vector of exogenous disturbances (possibly forces and torques), F_c is a continuous, distributed controlled force field (an available option in only some special applications), and F_a represents controlled forces due to localized actuation;

$$F_a(t, z) = \sum_{j=1}^k b_j(z)u_j(t) = B_0u(t). \quad (2.3)$$

The actuator influence functions $b_j(z)$ are highly localized in Ω and can be approximated by Dirac delta functions. We assume that a finite number p of measurements can be made as:

$$y(t) = C_0w + C'_0 \frac{\partial w}{\partial t} \quad (2.4)$$

where $y(t)$ is a p -vector. The operators $B_0 : \mathbb{R}^m \rightarrow \mathcal{H}_0$, $C_0 : \mathcal{H}_0 \rightarrow \mathbb{R}^p$, and $C'_0 : \mathcal{H}_0 \rightarrow \mathbb{R}^p$ are bounded.

A natural assumption for structural problems [1] is that A_0 is self-adjoint with compact resolvent and discrete (real) spectrum which is bounded from below. The system state can then be considered as an element of a Hilbert space $\mathcal{H} = D(A_0^{\frac{1}{2}}) \times \mathcal{H}_0$ with the energy norm

$$\|x\|_E^2 = \langle w, A_0w \rangle_0 + \langle m\dot{w}, \dot{w} \rangle_0 \quad (2.5)$$

where the first term represents potential energy and the second term is kinetic energy. Thus the (abstract) *state space model* can be written

$$\begin{aligned} \dot{x}(t, z) &= Ax(t, z) + Bu(t) \\ y(t) &= Cx(t, z) \end{aligned} \quad (2.6)$$

where

$$A = \begin{bmatrix} 0 & I \\ -A_0 & -D_0 \end{bmatrix}, \quad B = \begin{bmatrix} 0 \\ B_0 \end{bmatrix}, \quad C = [C_0, C'_0]. \quad (2.7)$$

For the elastic dynamics of space structures, there is always some (possibly small) damping D_0 appearing in (2.1) which causes A to be dissipative. Thus the criteria of the Hille-Yoshida-Phillips theorem [6] are satisfied and A generates a C_0 -semigroup with an operator which

we write suggestively as e^{At} . Moreover, such models are 'hyperbolic' [1] in the sense that the semigroup is a contraction, i.e., $\|e^{At}\| \leq 1$ and all but the zero frequency poles are only slightly damped; $\|e^{At}\| \leq e^{-\delta t}$ for some small $\delta > 0$. We remark that some popular models for structural elements such as beams with material damping may not fit in this framework [7, 8]. However, this framework includes models appropriate for considerations of wave-like dynamics which propagate causally in the spatial domain. For such models, the question of how to compute controls $u(t)$ and system response $x(t)$ focuses on the so-called *weak solution* of (2.6);

$$x(t, z) = e^{At}x(0, z) + \int_0^t e^{A(t-\sigma)}Bu(\sigma)d\sigma. \quad (2.8)$$

PDE's encountered in generic models of the form (2.1) represent the time evolution of certain physical systems and are typically of either *hyperbolic* or *parabolic* type. To clarify terminology consider the system of first-order, partial differential equations defined for $t \geq 0$ and $0 \leq z \leq L$

$$E \frac{\partial w}{\partial t} = \tilde{F} \frac{\partial w}{\partial z} + \tilde{H}w, \quad w \in R^n. \quad (2.9)$$

If E is nonsingular, then (2.9) can be written

$$\frac{\partial w}{\partial t} = F \frac{\partial w}{\partial z} + Hw \quad (2.10)$$

where $F = E^{-1}\tilde{F}$, $H = E^{-1}\tilde{H}$. If F has only real eigenvalues and a complete set of eigenvectors, then the system is said to be *hyperbolic* (see, for example, Zauderer [9]). If there are multiple real eigenvalues and less than a complete set of eigenvectors, then the system is of (partial) *parabolic* type. If all of the eigenvalues are complex, the system is of *elliptic* type. Systems with complex eigenvalues are not causal and will not be considered further.

If E is singular, (2.9) can give rise to mixed systems of all types. Our interest in this case will be limited to purely parabolic systems of the type

$$\frac{\partial w}{\partial t} = G \frac{\partial^2 w}{\partial z^2} + F \frac{\partial w}{\partial z} + Hw \quad (2.11)$$

which commonly arise in engineering problems.

In addition to equations (2.9) or (2.11), there are associated initial and boundary conditions. For equation (2.9), these conditions take the general form

$$\begin{aligned} \text{initial conditions} \quad & w(z, 0) = f(z) \\ \text{boundary conditions} \quad & \Sigma_1 w(0, t) + \Gamma_1 w(L, t) = g(t) \end{aligned} \quad (2.12)$$

where $\dim(g) = \dim(w)$; and for equation (2.11), they take the general form

$$\begin{aligned} \text{initial conditions} \quad & w(z, 0) = f(z) \\ \text{boundary conditions} \quad & \Sigma_1 w(0, t) + \Sigma_2 \frac{\partial w}{\partial z}(0, t) + \Gamma_1 w(L, t) + \Gamma_2 \frac{\partial w}{\partial z}(L, t) = g(t) \end{aligned} \quad (2.13)$$

where $\dim(g) = 2\dim(w)$.

It is well known that the coefficient matrices in (2.12), (2.13) must satisfy certain constraints if the problem formulation is to be well-posed. In the hyperbolic case (equations (2.9) and (2.12)), these constraints essentially require that the boundary conditions be compatible with the wave directions.

2.1.1 Frequency Response Models for Elastic Structures

The class of models discussed above captures the time response of causal, linear systems arising in the modeling of flexible structures. For the computation of optimal control laws for such systems we are concerned with models for the effective system frequency response. A complete modeling approach is described in [2] which we summarize in the next few paragraphs.

The complete system transient response can be characterized in the frequency domain in terms of the superposition of the forced response (modeled via a transfer function) and the free response (modeled via a Green's function). To illustrate the approach consider a hyperbolic model in one space dimension $0 \leq z \leq L$,

$$\frac{\partial x(t, z)}{\partial t} = F \frac{\partial x(t, z)}{\partial z} + Hx(t, z) + Ev(t, z) \quad (2.14)$$

subject to boundary conditions

$$\Sigma_1 x(t, 0) + \Gamma_1 x(t, L) = Df(t), \quad (2.15)$$

and initial conditions

$$x(0, z) = x^0(z) \in \mathcal{H}^n(0, L). \quad (2.16)$$

Here, x is an n -vector valued state $x \in \mathcal{H}^n(0, L)$, $v \in \mathcal{H}^\ell(0, L)$ is an ℓ -vector valued distributed disturbance, f is m -vector valued boundary interactions, F , H are real $n \times n$ matrices with F nonsingular and diagonalizable [9], and Σ_1 , Γ_1 are $n \times n$ matrices. After taking Laplace transforms in the temporal variable t , we obtain

$$\hat{X}(s, z) = \int_0^L G_r(s, z, w) \hat{M}(s, w) dw + H_{BC}(s, z) \hat{F}(s) \quad (2.17)$$

where

$$\hat{M}(s, z) = x^0(w) - C \hat{V}(s, w),$$

and \hat{X} , \hat{V} , \hat{F} are the Laplace transforms of x , v , f respectively. The function $G_r(s, z, w)$ is the *Green's function* [10, 11] for (2.14), (2.15) and $H_{BC}(s, z)$ is a transfer function from boundary interactions to state. Since in most cases of practical interest the control of flexible structures will be effected by actuators whose influence functions are highly localized, we have formulated our model with boundary control only.

The system *transfer function* with respect to boundary control has the form

$$H_{BC}(s, z) = N(s, z)D \quad (2.18)$$

where

$$\begin{aligned} N(s, z) &= \Phi(s, z) [\Sigma_1 + \Gamma_1 \Phi(s, L)]^{-1}, \\ \Phi(s, z) &= e^{[F^{-1}(sI - H)z]}. \end{aligned} \quad (2.19)$$

The Green's function for (2.14), (2.15) is the solution to

$$\frac{\partial G_r(s, z, w)}{\partial z} = F^{-1} [sI - H] G_r(s, z, w) + I_n \delta(z - w) \quad (2.20)$$

subject to the boundary conditions

$$\Sigma_1 G_r(s, 0, w) + \Gamma_1 G_r(s, L, w) = 0 \quad (2.21)$$

where $\delta(\cdot)$ is the Dirac delta function [10], [11]. Further discussion of the computation of the required Green's functions is discussed in [2].

For the case of a parabolic model we begin with the system equations in the form,

$$\frac{\partial x(t, z)}{\partial t} = G \frac{\partial^2 x(t, z)}{\partial z^2} + F \frac{\partial x(t, z)}{\partial z} + Hx(t, z) + Ev(t, z) \quad (2.22)$$

subject to $2n$ boundary conditions

$$\Sigma_1 x(t, 0) + \Sigma_2 \frac{\partial x(t, 0)}{\partial z} + \Gamma_1 x(t, L) + \Gamma_2 \frac{\partial x(t, L)}{\partial z} = Df(t), \quad (2.23)$$

and n initial conditions

$$x(0, z) = x^0(z) \in \mathcal{H}^n(0, L). \quad (2.24)$$

Let $\Sigma = [\Sigma_1, \Sigma_2]$ and $\Gamma = [\Gamma_1, \Gamma_2]$ —each $2n \times 2n$ real matrices. The transfer function from boundary control is then of the form

$$H_{BC}(s, z) = M(s, z)D, \quad (2.25)$$

where

$$\Lambda(s) \equiv \begin{bmatrix} 0_n & I_n \\ -G^{-1}(H - sI_n) & -G^{-1}F \end{bmatrix}, \quad (2.26)$$

$$\Phi(s, z) \equiv e^{\Lambda(s)z}, \quad (2.26)$$

$$M(s, z) = [I_n, 0]\Phi(s, z)[\Sigma + \Gamma\Phi(s, L)]^{-1}. \quad (2.27)$$

Hybrid Models for Flexible Space Structures. In most applications, models for the dynamics of flexible structures involve interaction between various elastic and rigid components. In the particular case of flexible structures associated with large space structures, the potential topological configurations can be quite complex. Various elements such as beams, truss structures, cables, membranes, etc., may have dominant distributed parameter effects. Typically a central body or bodies represent large concentrations of mass with respect to the overall low mass density of the flexible structure. These are most effectively represented by lumped parameter models of their rigid body dynamics. Hybrid models can provide an effective tool for analysis of dynamics of vibrations and their effect on small angle motions for complex space platforms.

To assemble the hybrid model we consider the Distributed Parameter System (DPS) to be modeled as either the hyperbolic or parabolic (or mixed) cases which, as we have seen, can be expressed in the frequency domain in the form

$$\hat{X}_d(s, z) = \int_0^L G_r(s, z, w) \hat{M}(s, w) dw + H_{BC}(s, q) \hat{F}_d(s) \quad (2.28)$$

where

$$\hat{M}(s, w) = x_d^0(w) - E\hat{V}(s, w). \quad (2.29)$$

Clearly, (2.28)-(2.29) can represent a disjoint collection of distributed elements such as beams, cables, etc.

The Lumped Parameter System (LPS) component model are combined into a single LPS state model of the form

$$\dot{x}_\ell(t) = A_\ell x_\ell(t) + B_\ell f_\ell(t), \quad x_\ell^0 = x_\ell(0) \quad (2.30)$$

with $x_\ell \in R^{N_\ell} \equiv \mathcal{X}_\ell$ a finite dimensional real space. By taking Laplace transforms in (2.30), we write (analogous to (2.28))

$$\hat{X}_\ell(s) = R_\ell(s)x_\ell^0 + H_\ell(s)\hat{F}_\ell(s), \quad (2.31)$$

where $R_\ell(s) = [sI_{N_\ell} - A_\ell]^{-1}$ is the resolvent for the (matrix) operator A_ℓ and $H_\ell(s) = R_\ell(s)B_\ell$.

Finally, the interconnection of component systems is resolved through a topological constraint relation consisting of $m = m_d + m_\ell$ linear equations;

$$f(t) + T_1 x_d(t, 0) + T_2 x_d(t, L) + T_3 x_\ell(t) = Ku(t) \quad (2.32)$$

where $u(t)$ is a k -vector of control inputs to the hybrid system, T_1, T_2 are $m \times N_d$, T_3 is $m \times N_\ell$, and K is $m \times k$ real matrices. The hybrid model state space consists of elements of the form

$$x(t, z) = \begin{pmatrix} x_\ell(t) \\ x_d(t, z) \end{pmatrix} \quad (2.33)$$

which are $N = N_d + N_\ell$ -valued functions of $z \in [0, L]$, $t > 0$. The resulting model has the form

$$\hat{X}(s, z) = \int_0^L \tilde{G}_r(s, z, w)\hat{M}(s, w)dw + \tilde{R}(s, z)x_\ell^0 + \tilde{H}_{BC}(s, z)\hat{U}(s), \quad (2.34)$$

where $\hat{M}(s, w)$ is given in (2.29). The complete system response is given in terms of the free response to initial conditions in the LPS state via an $N \times N_\ell$ matrix transfer function and the free response to initial conditions in the DPS state given by a $N \times N_d$ Green's function \tilde{G}_r ;

$$\tilde{R}(s, z) = \begin{bmatrix} I_{N_\ell} - H_\ell(s)\tilde{Q}_1(s) \\ -H_{BC}(s, z)\tilde{Q}_2(s) \end{bmatrix} T_3 R_\ell(s), \quad (2.35)$$

$$\tilde{G}_r(s, z, w) = \begin{bmatrix} -H_\ell(s)\tilde{Q}_1(s) \\ G_r(s, z, w) - H_{BC}(s, z)\tilde{Q}_2(s) \end{bmatrix} P(s, w) \quad (2.36)$$

where

$$\tilde{Q}(s) = [I_M + Q(s)]^{-1} = \begin{bmatrix} \tilde{Q}_1(s) \\ \tilde{Q}_2(s) \end{bmatrix}, \quad (2.37)$$

$$Q(s) = [T_3 H_\ell(s), T_1 H_{BC}(s, 0) + T_2 H_{BC}(s, L)], \quad (2.38)$$

$$P(s, w) = T_1 G_r(s, 0, w) + T_2 G_r(s, L, w). \quad (2.39)$$

The forced response is given by the transfer function from boundary control,

$$\tilde{H}(s, z) = \begin{bmatrix} H_t(s) & 0 \\ 0 & H_{BC}(s, z) \end{bmatrix} \tilde{Q}(s)K. \quad (2.40)$$

In the phase 1 effort we considered the transfer function models of several simple systems representative of vibration control problems. We would like to emphasize that the control methods we have considered and tested in Phase 1 are by no means limited to DPS applications. In fact we illustrate the computations required using a standard finite element model in one of the benchmark problems considered. The significant aspect of the modeling formulation above is in the fact that we *require* only frequency response models and therefore the computational approach is general enough to include a class of DPS large enough to encompass flexible space structure applications.

2.2 Control Synthesis via Wiener-Hopf Methods

A complete frequency domain design method for multi-input/multi-output (MIMO) systems based on a optimal Wiener-Hopf problem was first given by Youla et al [3] in 1976. The method described by Youla and his colleagues are very significant for control system design for several reasons. The method directly addresses several key design objectives and tradeoffs for closed loop control and uses the setting of Wiener-Hopf optimization to resolve tradeoffs. The formulation of the problem in the frequency domain permits both stabilization and system performance to be addressed in the same objective. This is accomplished by the characterization of an algebraic condition depending on the transfer function of the plant which must be satisfied by any closed loop controller which stabilizes this plant. Then performance objectives can be defined in a frequency dependent setting without regard to stability. The solution of the resulting optimal control problem is obtained by solving a set of Wiener-Hopf problems subject to the constraint that the controller must stabilize the plant.

Youla's approach focuses on a specific control architecture displayed in Figure 2.1 of practical significance in a wide variety of control problems where $P(s)$ is an $n \times m$ plant transfer function and $F(s)$ is $n \times n$ and models sensor measurement dynamics. The incorporation of $n \times n$ feedforward transfer function $L(s)$ is included to permit compensation for load disturbances which can be sensed prior to their effect being observed on the plant. In cases where plant delays are appreciable this feature may add substantially to the ability to compensate for output loads. The design model proposed offers several significant alternatives for control of flexible space structure control where a variety of sensors may be available which can predict dynamic loading under varying environmental conditions such as thermal gradients encountered with exposure to sun light.

Exogenous disturbances d , sensor noises n_t, n_f , and desired set points u are modeled as zero mean, wide sense stationary random processes and are therefore characterized by their respective power spectral densities; $G_d(s)$, $G_{n_t}(s)$, $G_{n_f}(s)$, $G_u(s)$. Notice that no assumption is made about the form of the controller $C(s)$ except the obvious dimensions: $m \times n$.

A significant feature of the Youla method is the algebraic parametrization of *all* stabilizing compensators for a given plant and sensor combination. Following [3] we will call the combination of P and F *admissible* [3] if each transfer function is free of hidden modes and

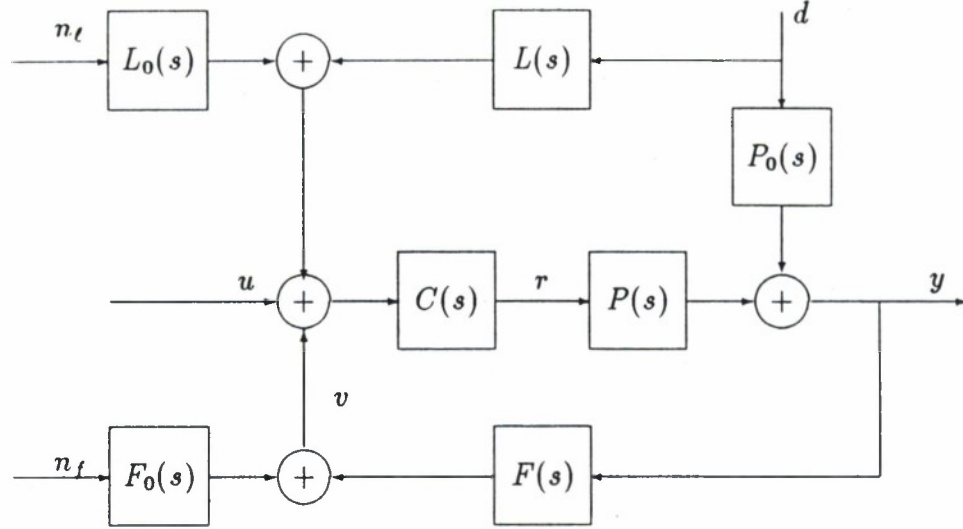


Figure 2.1: Multiloop Control Configuration for Wiener-Hopf Design

if the combination does not introduce cancellation of poles and zeros in the Closed Right Half Plane (\mathbf{C}_+). (This amounts to a requirement for stabilizability and detectability of the plant model.) Given that P and F are admissible let

$$F(s)P(s) = D_\ell^{-1}(s)N_\ell(s) = N_r(s)D_r^{-1}(s)$$

where N_ℓ , D_ℓ (resp. N_r , D_r) are left (right) coprime factorizations. As a result there will always exist a pair of polynomial matrices $X(s)$ and $Y(s)$ such that [12, 4]

$$D_\ell(s)X(s) + N_\ell(s)Y(s) = I.$$

Then the closed loop system is asymptotically stable if and only if the controller is of the form

$$C(s) = [Y(s) + D_r(s)K(s)][X(s) - N_r(s)K(s)]^{-1}. \quad (2.41)$$

where K is *any* $m \times n$ real rational matrix, analytic in \mathbf{C}_+ and $\det[X(s) - N_r(s)K(s)] \neq 0$. Thus *all* stabilizing controllers can be expressed in terms of a “stable parameter”, $K(s)$.

With the above parameterization in hand synthesis can be based on an optimal control problem which attempts to minimize tracking error $e = u - y$ subject to a power-like constraint on the control r . Thus let¹

$$J_t = \frac{1}{2\pi i} E \left\{ Tr \int_{-\infty}^{i\infty} e(s)e_*(s)ds \right\} \quad (2.42)$$

subject to a constraint

$$J_s = \frac{1}{2\pi i} E \left\{ Tr \int_{-\infty}^{i\infty} P_s(s)r(s)r_*(s)P_{s*}(s)ds \right\}, \quad (2.43)$$

¹We use the notation $u_*(s) = u^T(-s)$, E denotes expectation, and Tr denotes trace.

where $P_s(s)$ is the transfer function from the control signal r to those sensitive plant modes which must be protected against saturation. The resulting optimal control problem is to find the controller (i.e. the parameter $K(s)$) such that the cost

$$J = J_t + kJ_s \quad (2.44)$$

is minimized where $K(s)$ is allowed to vary over all stable transfer functions of appropriate dimensions and $k > 0$ is a real parameter which plays the role of a Lagrange multiplier and effectively permits tradeoff between tracking and saturation.

A complete solution can be obtained by the following procedure:

Wiener-Hopf Design Procedure (Youla's Method)

Step 1 Obtain coprime factorizations

$$F(s)P(s) = D_t^{-1}(s)N_t(s) = N_r(s)D_r^{-1}(s) \quad (2.45)$$

Step 2 Compute spectral factorizations

$$D_{r*}[P_*P + kQ]D_r = \Lambda_*\Lambda \quad (2.46)$$

$$D_tG_eD_{t*} = \Omega\Omega_* \quad (2.47)$$

where Ω, Λ are analytic together with their inverses in CRHP and

$$G_e = G_u + (FP_o + L)G_d(FP_o + L)_* + F_oG_nF_{o*} + L_oG_{n*}L_{o*}, \quad (2.48)$$

is the combined power spectral density of the exogenous inputs to the control system.
2

Step 3 Find a solution $X(s)Y(s)$ to the Diophantine equation;

$$D_t(s)X(s) + N_t(s)Y(s) = I_p. \quad (2.49)$$

Step 4 Compute the transfer function

$$Z(s) = D_{r*}P_*[G_u + P_oG_d(FP_o + L)_*]D_{t*} \quad (2.50)$$

and the stable parameter³

$$K(s) = \Lambda^{-1} \left(\{\Lambda_*^{-1}Z\Omega_*^{-1}\}_+ + \{\Lambda D_r^{-1}Y\Omega\}_- \right) \Omega^{-1} - D_r^{-1}Y. \quad (2.51)$$

Then the optimal controller has transfer function given by the parametric formula (2.41).

²We remark that the computations of the spectral factors in (2.46) (resp. (2.47)) effectively replace the computational step of solving a Riccati matrix equation for the control (resp. filter) problem typically encountered in modern state-space methods for control design. For systems with distributed parameter models the Riccati equation is a PDE and therefore difficult to solve by standard methods.

³A rational (matrix) function has a (partial fraction) expansion $A(s) = \{A(s)\}_+ + \{A(s)\}_- + \{A(s)\}_\infty$ where $\{.\}_+$ (resp. $\{.\}_-$) is the part analytic in $\Re s > 0$ —the causal part ($\Re s < 0$ —the anti-causal part) and $\{.\}_\infty$ is the part associated with poles at infinity.

The design method permits direct evaluation of control design tradeoffs in terms of certain critical frequency response functions. From the control architecture shown in Fig. 2.1 we can readily derive the closed loop frequency responses as

$$y = PCS(u - F_o n_f - L_o n_\ell) + [P_o - (FP_o + L)CS]d \quad (2.52)$$

$$r = CS[u - F_o n_f - L_o n_\ell - (FP_o + L)d] \quad (2.53)$$

$$e = (I - PCS)u + PCS(F_o n_f + L_o n_\ell) - [P_o - PCS(FP_o + L)]d \quad (2.54)$$

where the *system sensitivity operator*

$$S \equiv [I + FPC]^{-1}, \quad (2.55)$$

is a critical transfer function whose frequency response highlights the broadband action of the feedback control law. For the optimal control computed by the method outlined above the system sensitivity is given by

$$S = (X - N_r K)D_\ell, \quad (2.56)$$

a relation whose simplicity underlies the algebraic characterization of feedback design from the frequency response viewpoint.

The basis for resolving the engineering tradeoff of closed loop control action in terms of the conflicting requirements for stability, disturbance rejection, command tracking, and saturation avoidance is the application of Wiener-Hopf method for the solution of the optimization problem outlined above. It can be easily shown that the optimal performance objectives J_t and J_s are readily computed from the frequency domain solution above from the following formulae:

$$J_t = \frac{1}{2\pi j} \int_{-j\infty}^{j\infty} \text{Tr } \Phi_t(j\omega) d\omega, \quad (2.57)$$

$$J_s = \frac{1}{2\pi j} \int_{-j\infty}^{j\infty} \text{Tr } \Phi_s(j\omega) d\omega, \quad (2.58)$$

where

$$\Phi_t = (I - PR)G_u(I - PR)_* + (PR)G_1(PR)_*, \quad (2.59)$$

$$\Phi_s = QRG_e R_*, \quad (2.60)$$

$$G_1 = F_o G_{n_f} F_{o*} + L_o G_{n_\ell} L_{o*}, \quad (2.61)$$

$$P_d = FP_o + L, \quad (2.62)$$

$$R = (Y + D_r K)D_\ell. \quad (2.63)$$

Thus the design method proceeds by resolving the tradeoff between tracking performance (requiring high loop gains) and saturation limitation of the critical plant modes (which will limit loop gains) by direct implementation of the composite cost relative scale factor k in (2.44) which plays the role of a Lagrange multiplier.

Remarks on the Extension of Youla's Methods. Recent activity in the theory of robust control system design methods has focused on the solution of certain minimax or worst case design problems described in terms of frequency response models and frequency dependent model uncertainty [12]. Solutions have been obtained for a class of H^∞ optimal control design problems by extending the application of the algebraic characterization of the class of stabilizing controllers for a given plant given in (2.41). In Youla's original work the notion of coprime factorization was based on the natural choice for rational transfer functions: the factorization was with respect to the ring of polynomials. This paradigm ultimately limited the popularity of Youla's original design methods since for all but rather simple systems the factorization steps became computationally cumbersome.

The modern approach described by Vidyassagar [12] extends Youla's characterization of all stabilizing controllers by introducing the idea of obtaining coprime factorizations of transfer functions over the *ring of stable, rational transfer functions*. It is shown in [12] that the set of all transfer functions with poles contained in a half plane form an algebraic ring with respect to the usual operations of addition and multiplication. This characterization is of practical importance for control system design since one can now further constrain the optimal control computation so that a prescribed degree of stability will be obtained in the closed loop. In general, the extension of this algebraic characterization of the class of stabilizing controllers for irrational transfer functions is incomplete, but for the special class of irrational transfer functions arising in flexible structure control the essential characterization is now complete.

2.3 Wiener-Hopf Design for A Class of Irrational Transfer Functions

The formal extension of the algebraic computations for stabilizing and optimal control synthesis in the frequency domain is an area of active research [12, pp. 357]. In this section we summarize available results for a limited class of 'pseudo-meromorphic' transfer functions which include most linear, time-invariant models arising in control of flexible space structures [2]. We refer the reader to recent work of Baras for proofs and details [13, 14].

The results of Baras extend the critical constructions required for Wiener-Hopf design to the class of 'pseudo-meromorphic' transfer functions, denoted as \mathcal{A}_m^∞ , containing transfer functions

$$G \in H^\infty(C_+)$$

where C_+ denotes the closed right half plane and H^∞ is the Hardy space of bounded analytic functions on C_+ . Such transfer functions have (weak) coprime factorizations over $M(\mathcal{A}_m^\infty)$ ⁴

$$T(i\omega) = N_r(i\omega)D_r^{-1}(i\omega) = D_\ell^{-1}(i\omega)N_\ell(i\omega)$$

in the sense that N_r, D_r, D_ℓ, N_ℓ are in $H^\infty(C_+)$ provided that D_ℓ, D_r are inner [4, pp. 635].

Alternately, we say that $N(s)(p \times m)$, $D(s)(m \times m)$ are *strongly coprime* if there exist $\delta > 0$ such that

$$\|N(s)x\| + \|D(s)x\| \geq \delta > 0$$

⁴Let $M(\mathcal{A}_m^\infty)$ be the set of matrix transfer functions (of dimensions determined by the context) with elements in \mathcal{A}_m^∞ .

for all $x \in C^n$ and $s \in C_+$. Then the Carleson Corona theorem asserts that N, D are strongly coprime if and only if there exist X, Y in $H_{m \times m}^\infty$ such that

$$NY + DX = I_m.$$

Finally, the algebraic constructions required for the Wiener-Hopf control design method described above are extended by the following result [15, 16].

Theorem 1 Assume that $P, F, L, C \in \mathcal{A}_m^\infty$ and $FP \in \mathcal{A}_m^\infty$. Then all of the following hold.

1. The singularities of $[I + CFP]^{-1}FP$ are the zeros of $\det[D_\ell X + N_\ell Y]$.
2. There exist stabilizing controllers provided that N_ℓ, D_ℓ are *strong coprime*.
3. If N_r, D_r are strongly coprime then the closed loop system is BIBO (or exponentially) stable if and only if

$$C = (Y + D_r K)(X - N_r K)^{-1}$$

where K is any element of \mathcal{A}_m^∞ , such that $\det(X - N_r K) \neq 0$, analytic in $\Re s > 0$ ($\Re s \geq 0$), and X and Y are solutions of the Diophantine identities

$$D_\ell X + N_\ell Y = I.$$

Computational Requirements for Wiener-Hopf Methods For rational transfer functions the required computational steps outlined by Youla and his colleagues for Wiener-Hopf control can all be carried out over the ring of polynomials. More recently, the approach outlined by Vidyassagar [12] suggests that by performing computations over a *ring of stable transfer functions* (denoted S and including all functions rational, proper, and analytic in $C_+ \cup \{\infty\}$) the required computations can be directly supported in terms of state space realizations for the individual transfer functions. The key observation is that the collection of all proper, rational transfer functions with poles in C_+ form an algebraic ring which has the structure of a principal ideal domain (S).

Next we briefly outline several options for extending the required computations to \mathcal{A}_m^∞ . Just as in the rational transfer function case, the nonuniqueness of state space realizations for transfer functions may offer computational alternatives. Computational requirements for Wiener-Hopf synthesis include the following.

1. **Coprime Factorization.** For rational transfer functions the coprimeness condition for a pair (N, D) essentially amounts to a requirement for noncollocation of zeros for N and D . In general, irrational transfer functions may not have coprime factorizations [12]. In our studies the class of pseudo-meromorphic transfer functions includes most models for structural vibration control. Thus we have the existence of (strong) coprime factorizations in \mathcal{A}_m^∞ .
2. **Solution of Diophantine Relations.** Restricting attention to pseudo-meromorphic transfer functions gives the required existence of solutions to (2.49). Despite the potential lack of convergence of Euclidean division in \mathcal{A}_m^∞ Berenstein and Struppa [17] have

obtained explicit solutions to equations of the form (2.49) for (N, D) strongly coprime. The formulae obtained in [17] are nonalgebraic and extremely complex. Approximate solutions to the Bezout relations can also be obtained by sampling the Fourier response of the individual terms D_ℓ, N_ℓ, X, Y on a finite set of frequency samples. This reduces the computational problem to that of solving a set of simultaneous linear equations.

The insight from the algebraic approach to synthesis of stabilizing control [12] indicates that a particular solution X, Y to (2.49) is a *nominal stabilizing feedback control*; $K = YX^{-1}$. For most models of flexible structures arising in space applications the plant is nominally stable except for a finite number of poles either at the origin (associated with rigid body inertias) or in the right half plane. For such systems we have obtained direct methods for computing the required (stable) coprime factorizations. (See for example benchmark problem 2.)

3. **Spectral Factorization and Causal Projection.** In most cases arising in flexible structure control the resulting irrational transfer function model is meromorphic. In some simple cases the computational problems can often be reduced by the identification of an alternate state realization [18]. A more general approach is to use frequency sampling. Methods for matrix spectral factorization have been studied as alternatives to solving infinite dimensional Riccati equations by Davis [19] and Bennett [20] where a numerical algorithm is described. In the next section we describe results of testing a spectral factorization algorithm based on frequency response sampling.
4. **Linear Fractional Combinations.** All remaining constructions involve linear fractional transformations which can be readily supported via either explicit transfer function computations or frequency sampling.

Our conclusion from this survey is that frequency sampling offers an attractive alternative for the computational requirements of Wiener-Hopf synthesis and can readily be extended to transfer functions of pseudo-meromorphic type. The computational approach then obtains a *frequency sampled approximation* to the ideal, optimal controller for the given design problem and essentially provides a specification for such control. We remark that in contrast to state-space computations this approach decouples the realization of the controller from the computation of its response.

3 Phase 1 Project Results: Computation of optimal control for flexible structures by frequency sampling.

3.1 Frequency Response Design Method for Vibration Control

In the background material of section 2 we have described the basis for the design approach we have investigated in Phase 1 study for flexible space structures. Wiener-Hopf optimization is the basis for evaluating engineering tradeoffs with respect to the choice of required control law. For LQG type designs the tradeoff analysis from quadratic optimization results in a pair of feedback gain matrices. In the method we employ, the result is a complete

controller frequency response model. The Phase 1 effort has focused on the demonstration of the required frequency response modeling and control design computations for some simple benchmark problems in vibration control and isolation for flexible structures. We have demonstrated the feasibility of solving the Wiener-Hopf problem using frequency sampled data representation for:

1. *the plant model transfer function*, including the frequency response of the elastic structure to excitation by localized (point wise) actuation and possibly distributed disturbance excitation,
2. *the sensor/actuator model transfer function*, including provisions for both feedforward and feedback processing,
3. *the PSD of exogenous driving signals*, including sensor noises, output disturbances, and command inputs,
4. *control objectives*, including the specification of desired closed loop performance in terms of frequency dependent quadratic objective functions for both tracking and saturation avoidance.

In our benchmark problems we have considered both irrational transfer functions arising from standard model of a flexible beam and finite element model of a hybrid structure representing a problem of active vibration isolation. The method performs with success in both cases. Central to the success of the effort is a set of computational algorithms and an interactive environment for computation with frequency response models. One feature of the sampled frequency response computations is the requirement to choose a bandwidth and sampling interval for the model representation. Although guidance for these choices can be obtained from analysis of the transfer function models, it has been our experience that some fine tuning is desirable in applications. The interactive environment for frequency sampled computations supports this requirement.

3.2 Computational Algorithms for Frequency Domain Control Design

3.2.1 Coprime (stable) Factorization

Many flexible structure models involving hybrid dynamic models often include a finite number of unstable poles. In such cases the coprime factorization of the plant transfer function is a critical step which will guarantee the stability of the closed loop control system. The importance of the class of pseudo-meromorphic transfer functions is that the notion of *stable coprime factorization* can be extended to these systems.

By way of review, recall that a rational $p \times m$ strict proper transfer function, $P(s)$ has a minimal realization in terms of state space, matrix parameters (A, B, C)

$$P(s) = C(sI - A)^{-1}B, \quad (3.1)$$

where (A, B) is controllable and (A, C) is observable. Then the notion of coprime factorization with respect to a class of "stable" systems for which all members have poles within

an arbitrary (left) half plane, can be connected with state space computations as follows. Let S be the class of transfer functions with poles p_i such that $\Re p_i < \alpha$. Given a realization (A, B, C) for $P(s)$ then under the above conditions there exist S -stable coprime factorizations,

$$P = D_\ell^{-1} N_\ell = N_r D_r^{-1}, \quad (3.2)$$

which satisfy a doubly Diophantine relation,

$$\begin{bmatrix} Y_r & X_r \\ -N_\ell & D_\ell \end{bmatrix} \begin{bmatrix} D_r & -X_\ell \\ N_r & Y_\ell \end{bmatrix} = I_{p+m}. \quad (3.3)$$

It can be easily verified that the individual transfer functions $N_r, N_\ell, D_r, D_\ell, X_r, Y_r, N_\ell, D_\ell \in S$ can be obtained as:

$$\begin{aligned} N_\ell &= C(sI - A_o)^{-1} B, \\ D_\ell &= I - C(sI - A_o)^{-1} F, \\ N_r &= C(sI - A_c)^{-1} B, \\ D_r &= I - H(sI - A_c)^{-1} B, \\ X_r &= H(sI - A_o)^{-1} F, \\ Y_r &= I + H(sI - A_o)^{-1} B, \\ X_\ell &= H(sI - A_c)^{-1} F, \\ Y_\ell &= I + C(sI - A_c)^{-1} F, \end{aligned} \quad (3.4)$$

where the $n \times n$ matrices $A_c = A + BF$ and $A_o = A + HC$ are constructed by appropriate choice of the state feedback gain matrix F and the output injection matrix H so that the eigenvalues of A_c and A_o are contained in S .

The computations of coprime factorization can be readily extended to the class of models representing the dynamics of flexible structures under the following assumption. Let $P(s)$ be an irrational transfer function such that

$$P(s) = P_S(s) + P_{\mathcal{S}}(s) \quad (3.5)$$

where $P_S \in S \subseteq \mathcal{A}_m^\infty$ and $P_{\mathcal{S}}$ is rational and has (a finite number of) poles outside the half plane defining S ; i.e., $P(s)$ has only a finite number of "unstable" poles. In this case we can obtain the stable coprime factorization for $P(s)$ with respect to S as follows. Obtain a coprime factorization

$$P_{\mathcal{S}} = \tilde{N}_r \tilde{D}_r^{-1},$$

the unstable, rational term. This can be achieved by the state space constructions described above without reference to $P_{\mathcal{S}}$ —the irrational spectra of P . Then P has coprime factorization

$$P = N_r D_r^{-1} = [\tilde{N}_r - P_{\mathcal{S}} \tilde{D}_r] \tilde{D}_r^{-1}, \quad (3.6)$$

where N_r, D_r are S -stable. The separation of terms in (3.5) is readily carried out given $P(s)$ by computing the residues of the finite number of unstable poles contributing to $P_{\mathcal{S}}$. For most flexible structure problems the number of unstable poles is small arising from the interaction of elastic dynamics of the distributed structure with localized rigid body dynamics.

3.2.2 Solution of Diophantine Relations

The characterization of the class of all stabilizing controllers for a given rational transfer function, $P(s)$, as obtained by Youla and his coworkers, is given in terms of a coprime factorization $P = D_\ell^{-1}N_\ell$, and solution to a Diophantine relation (2.49). All stabilizing controllers $C(s)$ for $P(s)$ can then be described by the linear fractional transformation

$$C = [X - KN_\ell]^{-1}[Y - KD_\ell].$$

The characterization is algebraic for rational transfer functions and the computations can be effectively carried out by state space computations as described in the previous section.

For irrational transfer functions for which (strong) coprime factorizations exist we can readily obtain solutions to the Diophantine relation by frequency sampling. Rewriting (2.49) in the form

$$[D_\ell(s), N_\ell(s)] \begin{bmatrix} X(s) \\ Y(s) \end{bmatrix} = I_p, \quad (3.7)$$

it is clear that the required computation obtains a right inverse for the $p \times m + p$ matrix $[D_\ell(s), N_\ell(s)]$. This is readily obtained by frequency sampling using one of several standard numerical algorithms. A numerically stable approach is to use Singular Value Decomposition (SVD) of the $p \times m + p$ matrix obtained at each complex frequency sample s . The routine CSVDC contained in the Linpack software provides a direct way to obtain the right inverse (i.e., Moore-Penrose pseudo-inverse) from the SVD.

3.2.3 Spectral Factorization and Causal Projection

A critical computational requirement of the design method we have investigated is the requirement for solving two instances of Wiener-Hopf optimization based on frequency response data. Spectral factorization arises in optimal control and filtering problems by association with the solution of a Wiener-Hopf integral equation;

$$\int_0^\infty h(t - \tau)w(\tau)d\tau = f(t) \quad (3.8)$$

for $t > 0$ where, for example, $h(t)$ may be the covariance matrix of some noise process, $f(t)$ is a specified causal function, and $w(t)$, for $t > 0$ is the solution sought. The Wiener-Hopf technique solves (3.8) by the identification of a factorization of the Laplace transform

$$H(s) \equiv \int_{-\infty}^\infty h(t)e^{-st}dt,$$

of the form

$$H(s) = F(s)F^T(-s) \quad (3.9)$$

with the property that $F(s)$ is analytic together with its inverse in the closed right half plane, C_+ . For the case of $H(s)$ a rational (possibly matrix valued) transfer function, existence and uniqueness of the spectral factorization above follows under the conditions:

1. $\overline{H(s)} = H(\bar{s})$; i.e., $H(s)$ is the transform of a real-valued function $h(t)$.

2. $H(s) = H_*(s)$; i.e., $H(s)$ is "para-hermittian"
3. $H(s)$ is of normal rank; i.e., full rank almost everywhere in \mathbb{C} .
4. $H(i\omega)$ is positive, semi-definite for $\omega \in \mathbb{R}$.

More generally, (following the classical theory of Gohberg and Krein [21]) we have for the typical optimal filtering or control problem that $H(s) = I + G_*(s)G(s)$ where $G(s)$ is the transfer function of the system to be controlled and under the assumption that G_*G is:

1. positive, semi-definite for $s = i\omega$,
2. G_*G is the transform of a function which is both L_1 and L_2 ,

then the spectral factorization (3.9) exists and has the property

$$F(i\omega) - I \in \mathcal{F}(L_1^+ \cap L_2^+) \quad (3.10)$$

(where L_1^+ denotes those L_1 functions with positive support) and $\overline{F(s)} = F(\bar{s})$.

We are interested in obtaining a consistent, computationally efficient approximation for spectral factorization problems arising from transfer functions $G(s)$ belonging to the Hardy space $H^2 \cap H^\infty$ (which may include irrational cases). The approach we have in mind involves sampling and interpolation of the frequency response data $H(i\omega)$.

We will also consider the associated problem of *causal projection*;

$$\mathcal{P}_+ \{I + \int_{-\infty}^{\infty} f(t)e^{-i\omega t} dt\} \equiv I + \int_0^{\infty} f(t)e^{-i\omega t} dt. \quad (3.11)$$

Then, in the scalar case, if $F(s)$ is the scalar causal factor in (3.9) and $\Phi(s) = \ln H(s)$ we can write

$$\Phi(s) = \mathcal{P}_+ \{\Phi(s)\} + \mathcal{P}_- \{\Phi(s)\} \quad (3.12)$$

$$= \ln F(s) + \ln F_*(s) \quad (3.13)$$

so that the spectral factor can be obtained as $F(s) = \exp \mathcal{P}_+ \{\ln H(s)\}$. In the matrix case we employ a recursive algorithm for spectral factorization which is loosely based on a Newton-Raphson iteration for an associated Riccati equation. First, we consider computation of causal projection and spectral factorization in the scalar case by frequency sampling.

Spectral Factorization of Scalar Data Sequences. In the Phase 1 effort we have developed and tested computer algorithm for causal spectral factorization of frequency response samples based on an interpolation method of F. Stenger [22]. Roughly, Stenger's method offers an approximation of a function $g(\omega) \in \mathcal{F}(L_p)$ as an expansion

$$g^{(a)}(\omega) = \sum_{j=-\infty}^{\infty} g((j + \frac{1}{2})\Delta\omega) \chi_j(\omega) \quad (3.14)$$

where $\Delta\omega$ is a fixed sampling interval, and $\chi_j^{(a)}(\omega)$ is the j^{th} (approximate) characteristic function which approaches the ideal:

$$\chi_j(\omega) = \begin{cases} 1, & \text{for } \omega \in (j\Delta\omega, (j+1)\Delta\omega) \\ 0, & \text{else} \end{cases} \quad (3.15)$$

We summarize the theoretical basis for Stenger's method in the following theorems.

Theorem 2 Let $g \in \mathcal{F}(L_p)$. Then

$$g^{(a)}(\omega) \equiv \sum_{j=-\infty}^{\infty} g((j + \frac{1}{2})\Delta\omega) \chi_j(\omega) \quad (3.16)$$

approximates g in the sense that $\|g - g^{(a)}\|_p \rightarrow 0$ as $(\Delta\omega, k) \rightarrow (0+, 1-)$ where the approximate characteristic functions are

$$\chi_j(\omega) = \frac{1}{2\sqrt{k}} [1 + k\phi_j(\omega)], \quad (3.17)$$

and

$$\phi_j(\omega) = \text{sn} \left[\frac{2K}{\pi i} \log \left(\frac{\omega - (j+1)\Delta\omega}{\omega - j\Delta\omega} \right) - K + iK', k \right]. \quad (3.18)$$

Here we use the standard notation for the elliptic functions with parameter k , $0 \leq k < 1$; viz.,

$$z = \text{sn}[u, k]$$

if and only if

$$u(z) = \int_0^z \frac{dt}{\sqrt{(1-t^2)(1-k^2t^2)}}, \quad (3.19)$$

$$K(k) = u(1), \quad \text{and} \quad K' = K(\sqrt{1-k^2}). \quad (3.20)$$

We remark that the characteristic function $\chi_j(\omega)$ given in (3.17) has the following properties [22]:

1. for $\omega \in (j\Delta\omega, (j+1)\Delta\omega) \Rightarrow \chi_j(\omega) \in [(k^{1/2} + k^{-1/2})/2, k^{-1/2}]$,
2. for $\omega \in \Re - [j\Delta\omega, (j+1)\Delta\omega] \Rightarrow \chi_j(\omega) \in [0, (k^{-1/2} - k^{1/2})/2]$.

Theorem 3 The characteristic function $\chi_j(\omega)$ has the explicit representation

$$\chi_j(\omega) = \sum_{m=-\infty}^{\infty} \left\{ \frac{r_m}{\omega - p_m^{(j)}} + \frac{\bar{r}_m}{\omega - \bar{p}_m^{(j)}} \right\} \quad (3.21)$$

where the poles

$$p_m^{(j)} = (j + \alpha_m)\Delta\omega \quad (3.22)$$

and residues

$$r_m = -\frac{\pi\omega}{4\sqrt{k}K} q^m \alpha_m^2 \quad (3.23)$$

depend on the parameters

$$\alpha_m = \frac{1}{1 - iq^m} \quad (3.24)$$

$$q = \exp[-\pi \frac{K'}{K}] = \exp[-\frac{\pi}{K(k)} \int_0^1 \frac{dt}{\sqrt{(1-t^2)(1-(1-k^2)t^2)}}]. \quad (3.25)$$

We remark that $(p_m^{(j)}, r_m)$ corresponds to the anti-causal (right half plane) poles and residues of χ_j while $(\bar{p}_m^{(j)}, \bar{r}_m)$ are causal. This motivates the following result.

Theorem 4 Given $g(\omega) \in \mathcal{F}(L_p)$ the causal projection of $g(\omega)$, $\mathcal{P}_+ \{g\}$, can be obtained in the limit as follows,

$$\begin{aligned} g_+^{(a)} &= \lim_{(\Delta\omega, k) \rightarrow (0+, 1-)} \sum_{j=-\infty}^{\infty} g((j + \frac{1}{2})\Delta\omega) \mathcal{P}_+ \{\chi_j(\omega)\} \\ &= \lim_{(\Delta\omega, k) \rightarrow (0+, 1-)} \sum_{j=-\infty}^{\infty} g((j + \frac{1}{2})\Delta\omega) \sum_{m=-\infty}^{\infty} \frac{\bar{r}_m}{\omega - \bar{p}_m^{(j)}}. \end{aligned} \quad (3.26)$$

Then $\|g_+^{(a)}(\omega) - \mathcal{P}_+ \{g(\omega)\}\|_p \rightarrow 0$ as $(\Delta\omega, k) \rightarrow (0+, 1-)$.

Now assume that the scalar function $h(\omega) \in \mathcal{F}(L_1 \cap L_2)$ is positive real and thus has a spectral factorization $h(\omega) = f(\omega)\overline{f(\omega)}$ where $f(\omega)$ is the unique causal factor. We can extend the above causal projection computation via logarithmic transformation of the data as follows.

Theorem 5 Let $h(s)$ have the above properties, then the spectral factorization $h(s) = f(s)\overline{f(s)}$ exists and is unique where $f(s)$ and $1/f(s)$ are both analytic in \mathbb{C}_+ . Then the approximation

$$f^{(a)}(\omega) = \exp\left[\sum_{j=-\infty}^{\infty} \ln h((j + \frac{1}{2})\Delta\omega) \mathcal{P}_+ \{\chi_j(\omega)\}\right] \quad (3.27)$$

with $\mathcal{P}_+ \{\chi_j(\omega)\}$ given as in (3.26) has the property $\|f^{(a)}(\omega) - f(\omega)\|_p \rightarrow 0$ for both $p = 1, 2$ as $(\Delta\omega, k) \rightarrow (0+, 1-)$.

By way of summary of the theoretical basis for the algorithm we have in mind we direct attention to the following formula for (approximate) causal projection:

$$\mathcal{P}_+ \approx \sum_{j=-\infty}^{\infty} g((j + \frac{1}{2})\Delta\omega) \sum_{m=-\infty}^{\infty} \frac{\bar{r}_m}{\omega - \bar{p}_m^{(j)}} \quad (3.28)$$

and for (approximate) causal spectral factorization:

$$f(\omega) \approx \exp\left[\sum_{j=-\infty}^{\infty} \ln h((j + \frac{1}{2})\Delta\omega) \sum_{m=-\infty}^{\infty} \frac{\bar{r}_m}{\omega - \bar{p}_m^{(j)}}\right] \quad (3.29)$$

where the sampling interval $\Delta\omega$ is small enough and $k < 1$ but close to 1. Substitution of the expressions (3.22)–(3.25) reveals the relation

$$\frac{\bar{r}_m}{\omega - \bar{p}_m^{(j)}} = \frac{-\pi q^m \bar{\alpha}^2}{4\sqrt{k}K[(\omega - (j + \frac{1}{2})\Delta\omega) + \frac{1}{2} + \bar{\alpha}_m]}, \quad (3.30)$$

so that an M^{th} order approximation to the projected characteristic function for sampling interval $\Delta\omega$ is

$$\mathcal{P}_+ \{ \chi_j^M(\omega) \} = \sum_{m=-M}^M \frac{\bar{r}_m}{\omega - \bar{p}_m^{(j)}} =: \varphi^+(\omega - (j + \frac{1}{2})\Delta\omega) \quad (3.31)$$

so that the computation of (3.28) (or (3.29)) for uniform sampling $\omega = \ell\Delta\omega$, $\ell = 0, \pm 1, \pm 2, \dots$, reduces to the discrete convolution of the data sequences $g((j + \frac{1}{2})\Delta\omega)$ (resp. $\ln h((j + \frac{1}{2})\Delta\omega)$) and $\varphi^+(\omega - (j + \frac{1}{2})\Delta\omega)$ for $j = 0, \pm 1, \pm 2, \dots$. This is efficiently implemented using FFT processing.

The summation (3.31) converges rapidly if the characteristic function is chosen carefully; i.e., if $k < 1$ and close to 1. Well known properties of elliptic integrals suggest that we compute (k, K) by first choosing $q < 1$, then

$$k = \left(\frac{\theta_2}{\theta_3} \right)^2 \quad \text{and} \quad K = \frac{\pi}{2} (\theta_3)^2$$

where

$$\theta_2 = 2 \sum_{n=1}^{\infty} q^{(n-1/2)^2} \quad (3.32)$$

$$\theta_3 = 1 + 2 \sum_{n=1}^{\infty} q^{n^2}. \quad (3.33)$$

For example, the choice $q = \frac{1}{2}$ obtains $k = 0.999994$ and $K = 7.11943$. In this case we found $M = 8$ sufficient for single precision computation on a VAX 11/750.

Spectral Factorization of Matrix Frequency Samples. For the general MIMO design problem typical of flexible space structure control problems the spectral factorization steps are required for matrix valued transfer functions. In Phase 1 effort we have implemented and tested a computer algorithm which operates on the frequency sampled data by a recursive procedure to obtain the spectral factor. The basis for the algorithm can be obtained by association of the spectral factorization with the solution of a Riccati equation arising in the context of a quadratic optimal control problem:

$$\min_{u \in \mathcal{U}_{ad}} \int_0^{\infty} \|u(t)\|^2 + \|y(t)\|^2 dt \quad (3.34)$$

subject to the linear, time-invariant system model

$$\dot{x}(t) = Ax(t) + Bu(t), \quad x(0) = x_0 \quad (3.35)$$

$$y(t) = Cx(t), \quad t \geq 0, \quad (3.36)$$

where we assume $[A, B, C]$ is a minimal realization for the transfer function $G(s) = C[sI - A]^{-1}B$. The optimal control is known to be a linear state feedback $u(t) = -K_{opt}x(t) = -B^T P x(t)$ where P is the unique, positive definite symmetric solution to algebraic (matrix) Riccati equation,

$$PA + A^T P - PB^T B P + C^T C = 0. \quad (3.37)$$

Standard algebraic manipulations based on (3.34)-(3.37) provide the spectral factorization relation [23, pp. 68] which we write

$$H(s) = I + G^T(-s)G(s) = F^T(-s)F(s) \quad (3.38)$$

where $F(s) = I + K_{opt}[sI - A]^{-1}B$ is the *causal spectral factor* of the positive real transfer function, $H(s)$.

The algorithm we employ was first suggested by Davis and Dickinson [19] and takes the form of a Newton-Raphson recursion for the spectral factor;

$$F_{n+1}(i\omega) := \mathcal{P}_+ \left\{ [F_n^*(i\omega)]^{-1} H(i\omega) [F_n(i\omega)]^{-1} \right\} F_n(i\omega), \quad (3.39)$$

where \mathcal{P}_+ is the *causal projection operator*. The recursion (3.39) can be implemented in a form which enhances its numerical properties and provides an effective computer algorithm;

$$[F_{n+1}]^{-1} := [F_n]^{-1} \left(I + \mathcal{P}_+ \left\{ [F_n^*]^{-1} H [F_n]^{-1} - I \right\} \right)^{-1}. \quad (3.40)$$

By initializing with F_0 (an $m \times m$ diagonal matrix) with diagonal elements equal to the spectral factors of the diagonal elements of H the second term of (3.40) remains a perturbation of the identity (since $[F_n^*]^{-1} H [F_n]^{-1} - I \rightarrow 0$) which regularizes the computations. The diagonal initialization guarantees that the first residual $[F_0]^{-1} H [F_0]^{-1}$ has ones on the diagonal and all off diagonal elements less than one in magnitude. The resulting numerical problem is well-conditioned.

The conceptual algorithm can be summarized in the following pseudo-code.

Algorithm for Matrix Causal Spectral Factorization

Given: An $m \times m$ matrix valued data sequence $H(\omega)$ defined on a set of uniformly sampled frequency points $\omega \in \Omega$ together with the property that at each ω the matrix $H(\omega)$ is positive semi-definite, symmetric.

Initialize:

$$F^{(0)}(\omega) := \text{diag}\{f_k(\omega), k = 1, \dots, m\}$$

where the scalar data sequences $f_k(\omega)$ are computed using (3.29) from the m diagonal data sequences of $H(\omega)$.

$$[F^{-1}(\omega)]^{(0)} := \text{diag}\{1/f_k(\omega), k = 1, \dots, m\}.$$

Repeat Until $(\|R^{(j)}(\omega)\| < \epsilon)$ where ϵ is a specified tolerance.

$$j := j + 1$$

$$[F^{-1}(\omega)]^{(j)} := [F^{-1}(\omega)]^{(j-1)} (I_m + \mathcal{P}_+ \{R^{(j-1)}(\omega)\})^{-1}$$

Stop

Issues in Design of Efficient Computer Code. The primary observation that permits the design of an efficient computer algorithm follows from the relation (3.31) so that, in effect, (3.28) or (3.29) are discrete convolution of infinite data sequences. In applications, the summations appearing in (3.28) or (3.29) will converge rapidly and can be approximated within any desired precision by finite sums. For example, in design of control laws for flexible structures it is assumed that the transfer function model for the structural flexure response to control actuation is *strictly proper* with effective system bandwidth ω_{BW} which is known a priori (even if the exact transfer function is not known). Modeling issues relative to the determination of ω_{BW} for control of flexible structures are considered in [24]. Once the model bandwidth ω_{BW} has been obtained, together with a choice of a frequency sampling interval $\Delta\omega$ then we compute the approximating sequence $\mathcal{P}_+ \{g(\omega)\}$ as

$$\mathcal{P}_+ \{g(\omega)\} = \sum_{j=-N_p}^{N_p} g((j + \tfrac{1}{2})\Delta\omega) \varphi_+(\omega - (j + \tfrac{1}{2})\Delta\omega), \quad (3.41)$$

where $N_p \Delta\omega = \omega_{BW}$. This is a convolution of two data sequences g, φ_+ of length $2N_p$.

Since in many applications these data sequences may be relatively long, an efficient implementation of the required convolution may be obtained using an FFT algorithm. The development of reliable computer code for FFT processing has been quite extensive and several efficient, portable, and reliable codes are available in the public domain [25]. We have found the Fortran routine FFT842, available in [25], an efficient alternative which offers support for the required complex valued, frequency response data sequences.

In some cases, we may wish to operate directly on data sequences obtained from measurements on physical systems. For such cases we must concern ourselves with potential numerical errors due to aliasing and Gibbs phenomenon [26]. For application to control system design we believe it is important to consider such applications in the development of a comprehensive computer code and we have included various standard data windows for weighting the data sequences for FFT based convolution.

One critical tradeoff in the development and testing of computer code to support the required computations for Wiener-Hopf control system design is storage requirements for the complex data sequences. In Phase 1 the focus has been on the development of a prototype computer code for testing the numerical algorithms as well as experimenting with the choice of bandwidth and data sampling. Thus we have made provisions for graphical plotting of the various data sequences as the algorithm proceeds. We have made explicit provisions for storing a number of data sequences which are useful primarily for debugging and testing the code. As a result the prototype code is a data storage intensive implementation of the method. One area where data storage can be efficiently used is in the implementation of the spectral factorization by consideration of several basic properties of the matrix data sequences. Since by assumption, the model (3.35)–(3.36) involves real, vector-valued functions, $u(t)$, $y(t)$, and $x(t)$, the transfer function matrix has the property $G(i\omega) = \overline{G(-i\omega)}$. By the construction (3.38) $H(\omega)$ is Hermitian, positive definite for each ω .

At the j^{th} iteration, the recursion is driven by a matrix, residual data sequence;

$$R^{(j)}(\omega) := F_j^{-T}(-\omega)H(\omega)F_j^{-1}(\omega) - I \quad (3.42)$$

Matrix Sequence	$X(\omega) = \overline{X(-\omega)}$	Hermittian
G	\times	
H	\times	\times
R	\times	\times
$\mathcal{P}_+ \{R\}$	\times	
F	\times	

Table 3.1: Properties of Matrix Data Sequences

which is also Hermittian for each ω . Table 3.1 summarizes the properties of the matrix data sequences encountered.

The fact that the data sequences involve transforms of real-valued processes permits computational savings of the order of $2N_p$ for each scalar sequence since, at the j^{th} iteration, we can obtain the required sequences by only computing $R^{(j)}(\omega)$, $F_j^{-1}(\omega)$ for $\omega > 0$. Let $R_{k\ell}^{(j)}(\omega)$ denote the $k \times \ell$ entry of the residual sequence at iteration j . Then the following holds;

$$\begin{aligned}
 \mathcal{P}_+ \{R_{k\ell}^{(j)}(\omega)\} &= R_{k\ell}^{(j)}(\omega) - \overline{\mathcal{P}_- \{R_{k\ell}^{(j)}(\omega)\}} \\
 &= R_{k\ell}^{(j)}(\omega) - \overline{\mathcal{P}_+ \{R_{k\ell}^{(j)}(-\omega)\}} \\
 &= R_{k\ell}^{(j)}(\omega) - \overline{\mathcal{P}_+ \{R_{\ell k}^{(j)}(\omega)\}},
 \end{aligned} \tag{3.43}$$

where we have used the facts that for any $x(\omega)$ with $x(\omega) = \overline{x(-\omega)}$, $\mathcal{P}_- \{x(\omega)\} = \overline{\mathcal{P}_+ \{x(-\omega)\}}$, and by construction of the residual matrix,

$$R_{k\ell}(-\omega) = \overline{R_{k\ell}(\omega)} = R_{\ell k}(\omega).$$

Thus we can construct the lower triangular part of $\mathcal{P}_+ \{R^{(j)}(\omega)\}$ directly from its upper triangular part. If $R^{(j)}(\omega)$ is $N \times N$ then we are required to compute causal projection using the convolution (3.41) for only $\frac{N(N+1)}{2}$ scalar data sequences to construct the required causal projection.

Finally, the computation (3.40) requires simultaneous solution of a set of N linear equations for each ω . This can be implemented efficiently using the routines CGESL and CGECO available in Linpack [27].

We have coded and tested the spectral factorization algorithm for several problems of both scalar and matrix types and including both rational and irrational spectrum. In the next section we described the results of these studies in detail. It is informative to monitor the convergence of the recursion (3.40) by examining the residual at each iteration in terms of two norms:

$$\begin{aligned}
 \max_ele(R^{(j)}) &:= \max_{\omega, k, \ell} \{R_{k\ell}^{(j)}(\omega)\} \\
 \max_tr(R^{(j)}) &:= \max_{\omega} \{tr(R_{k\ell}^{(j)}(\omega) R_{k\ell}^{(j)}(\omega))\}.
 \end{aligned}$$

START UP MENU AND STATUS	

CHOOSE A NUMBER BELOW.	
	CURRENT VALUE
1. INPUT BAND WIDTH.	100.00
2. INPUT NUMBER OF SAMPLE POINTS.	1024
3. PLOT P(S).	
4. START PROGRAM.	
5. RETURN TO MAIN MENU.	

Figure 3.1: An example of the start.up menu.

3.3 Development and testing the interactive software environment

3.3.1 Objectives of the prototype software environment

There were four main objectives to the design of the software environment: to support the frequency sampling analysis, to monitor the causal spectral factorization algorithm convergence, to resolve design trade-offs, and to provide a means to obtain desired output. Additionally, an efficient user interface consisting of a menu format with options grouped according to major functions was desired.

Frequency sampling analysis is concerned with evaluating the frequency responses of specific functions at discreet frequency values. The software environment was designed to perform uniform frequency sampling computations using a maximum of 1024 points. The program permits the user to select a bandwidth and a number of frequency samples for the computations in the start.up menu. In addition, after making these selections, the user can plot the plant transfer function, $P(s)$, to evaluate these choices. The start.up menu appears in figure 3.1.

Another objective of the software design was to allow the user to monitor the convergence of the spectral factorization algorithm. This algorithm uses an iterative approach to converge on the spectral factor. The results of the convergence, which are the maximum trace and maximum element of the residual and the number of iterations needed to converge, are displayed in a summary format, as seen in figure 3.2. The user can change the convergence threshold, epsilon, and the maximum number of iterations the program will perform before reaching epsilon, and then recompute the spectral factor if desired.

An important aspect in the design approach of this paper is the design tradeoff between tracking cost and saturation cost. The software environment enables the user to generate a curve of saturation cost versus tracking cost as a function of the parameter k . This curve can be seen in figure 3.3. With this plot, the user can choose a k value that corresponds to some maximum saturation level and a corresponding tracking cost, and then generate the

----- RESIDUAL COMPUTATION SUMMARY -----		
ITERATION NO.	MAX. ELEMENT	MAX. TRACE
0	0.9001E+00	0.7547E-02
1	0.3935E+00	0.7807E+00
2	0.1367E+00	0.2728E+00
3	0.1271E-01	0.2540E-01
4	0.1197E-03	0.2389E-03
5	0.7935E-06	0.8964E-06
EPSILON		0.1000E-05
MAXIMUM NUMBER OF ITERATIONS		11
NUMBER OF ITERATIONS TO CONVERGE ON EPSILON		5
CHOOSE AN INTEGER		
1. CHANGE EPSILON		
2. CHANGE MAX ITERATIONS		
3. RECOMPUTE SPECTRAL FACTOR		
4. CONTINUE PROGRAM		

Figure 3.2: Residual computation summary from MIMO case benchmark problem.

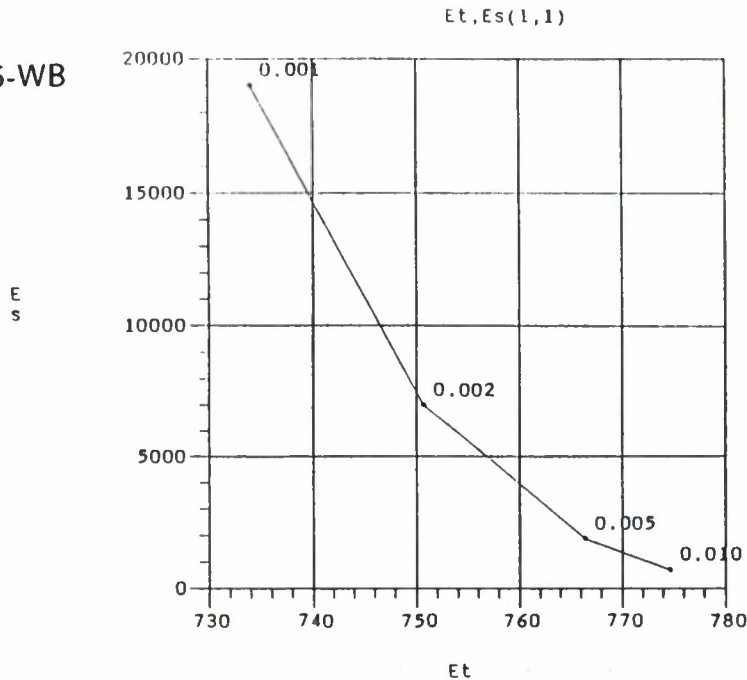


Figure 3.3: An example of a saturation cost vs. tracking cost plot.

design frequency response data with this k .

The final objective of the software was to provide a means for displaying and obtaining output of the frequency response data. Specific data relevant to control design were grouped into a plotting menu that appears in figure 3.4. These data can be plotted on the screen or as a hard copy in the various configurations shown in the plot type menu in figure 3.5. In addition, there is a feature in the main menu, that permits the user to save the data of figure 2.12 in a file for later plotting.

3.3.2 Testing and Benchmarks

The software was tested using four benchmark problems - a pinned- pinned beam with a torque at one end, a rigid stick on a cart subject to a disturbance, and a flexible stick on a cart subject to a disturbance in both SISO and MIMO cases. These benchmarks will be discussed in more detail in a following section, but a brief summary of the computational and storage requirements for these problems will be presented here.

The software was tested on a Micro VAX II, and the CPU time for each benchmark problem appears in Table 1. This time represents the actual CPU time required to perform all of the necessary computations required to calculate the frequency response of the optimum controller. As can be seen from the results, there was a substantial increase in CPU time for the MIMO case of the flexible stick on a cart, which is a reasonable result since this is a 2 by 2 matrix case whereas the other benchmarks were scalar cases.

The storage requirements for each benchmark also appear in Table 1. The frequency sampling approach is very data intensive, requiring storage of many arrays containing large numbers of elements. Most of the arrays typically contain 2048 elements in the scalar cases, and 8192 in the matrix case.

Additional observations of the results of the benchmarks show that accurate results of the

```
-----  
                        PLOTTING MENU.  
-----  
CHOOSE A NUMBER BELOW.  
  
1. XL(S)           8. K(S)  
2. YL(S)           9. S(S),I-S(S)  
3. OMEGA(S)        10. L(S)  
4. LAMBDA(S)       11. C(S)  
5. H(S)            12. ES,ET COST FUNCTIONS  
6. HH(S)           13. PO(S)  
7. Z(S)            14. RETURN TO MAIN MENU  
-----
```

Figure 3.4: The plotting menu.

```
-----  
                        PLOT TYPE MENU.  
-----  
CHOOSE A NUMBER BELOW.  
  
1. TYPE OF DATA REPRESENTATION---LINE  
2. REAL AND IMAGINARY VS. FREQUENCY.  
3. REAL VS IMAGINARY.  
4. MAGNITUDE AND PHASE VS FREQUENCY.  
5. RETURN TO PLOTTING MENU.  
-----
```

Figure 3.5: The plot type menu.

Benchmark	CPU Time	Storage Requirement
Pinned-Pinned Beam	6 min.	2.7 Meg
Rigid Stick on a Cart	5.5 min.	2.7 Meg
Flexible Stick on a Cart (SISO)	9.5 min.	2.7 Meg
Flexible Stick on a Cart (MIMO)	18 min.	5.1 Meg

Table 3.2: Benchmark computational times and storage requirements.

frequency response curves can be obtained using less than the maximum number of sample points (1024) which reduces the computational time and storage requirements substantially. Figure 3.6 shows the controller frequency response using 1024 points and figure 3.7 shows the same controller using only 256 points. The curves are very similar, but in both cases, the low frequency end of the response is under-sampled due to uniform sampling. However, by reducing the bandwidth, and thereby concentrating more of the sample points in the lower frequency region this under-sampling condition can be reduced.

3.3.3 Considerations for later versions

A review of the software design showed that a substantial decrease in memory storage can be realized by a reduction in the number and size of temporary storage arrays. Additionally, the size of some of the permanent arrays can also be reduced by rewriting the spectral factorization code. Furthermore, the program can be broken up into smaller segments that perform intermediate computations and then store pertinent data on disk, so that the memory requirement at any one time can be dramatically reduced. This, however, would increase the software run time.

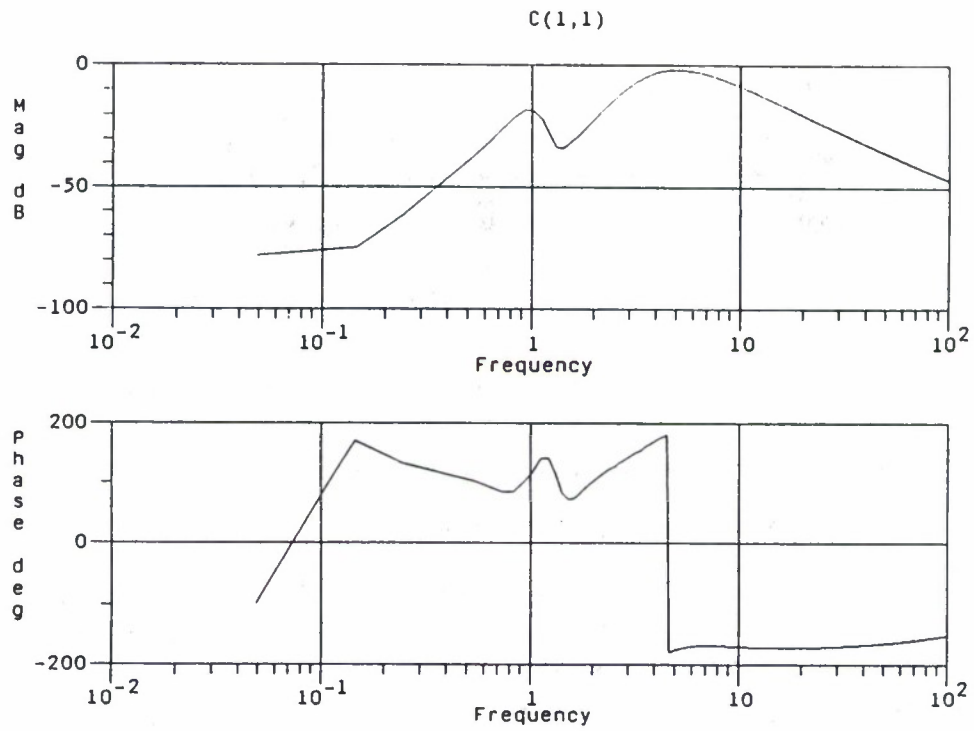


Figure 3.6: Controller frequency response with 1024 points.

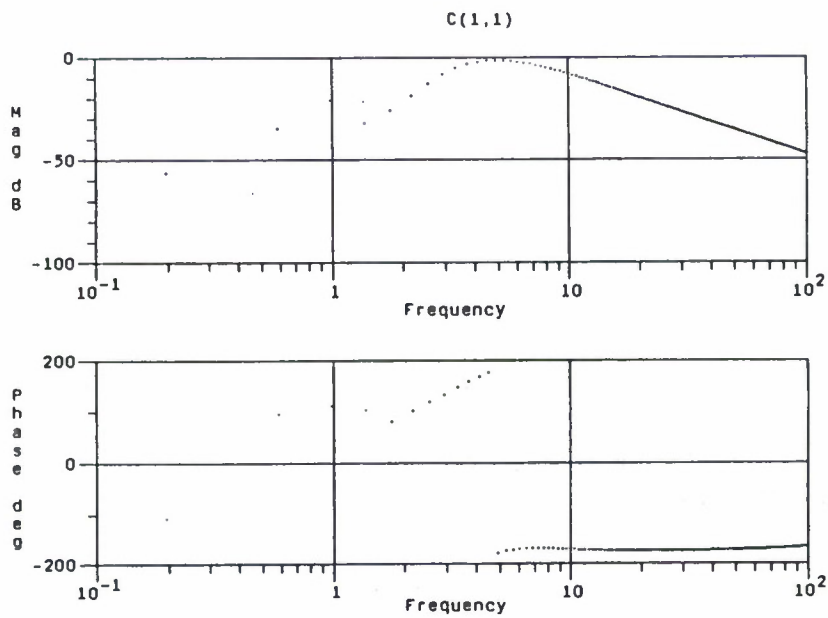


Figure 3.7: Controller frequency response with 256 points.

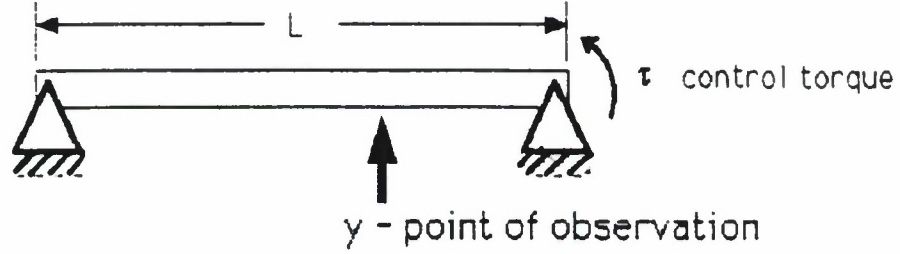


Figure 3.8: Pinned-Pinned Beam Control Problem.

3.4 Benchmark Problems Considered in Phase 1

3.4.1 Control of a pinned-pinned beam.

In this example we consider a control system design problem for a relatively simple structure with well known transfer function. Consider a Bernoulli-Euler beam model with "pinned-pinned" boundary conditions as shown in the figure. The beam lateral deformation is given by $y(t, z)$ with $0 \leq z \leq L$ and has dynamics described by the PDE;

$$\rho A \frac{\partial^2 y}{\partial t^2} - 2\zeta \sqrt{\rho A E I} \frac{\partial^3 y}{\partial t \partial z^2} + E I \frac{\partial^4 y}{\partial z^4} = 0, \quad (3.44)$$

with boundary conditions at $z = 0$,

$$y(t, 0) = 0,$$

(no lateral displacement)

$$\left. \frac{\partial^2 y}{\partial z^2} \right|_{z=0} = 0,$$

(no restraining moment), and at $z = L$,

$$y(t, L) = 0,$$

$$\left. \frac{\partial^2 y}{\partial z^2} \right|_{z=L} = \tau,$$

where the control moment is applied at the right hand end of the beam. In dimensionless form the PDE can be written,

$$\frac{\partial^2 y}{\partial t^2} - 2\zeta \frac{\partial^3 y}{\partial t \partial z^2} + \frac{\partial^4 y}{\partial z^4} = 0. \quad (3.45)$$

The transfer function for beam control is

$$P(s, z) = L^2 \frac{\sin \lambda_1 \sinh \lambda_2 \frac{z}{L} - \sin \lambda_1 \frac{z}{L} \sinh \lambda_2}{(\lambda_1^2 + \lambda_2^2) \sin(\lambda_1) \sinh(\lambda_2)}, \quad (3.46)$$

where

$$\lambda_1^2 = (-\zeta + i\sqrt{1 - \zeta^2})sL^2, \quad (3.47)$$

$$\lambda_2^2 = (\zeta + i\sqrt{1 - \zeta^2})sL^2, \quad (3.48)$$

L is the beam length, ζ is the damping factor, and $0 \leq z \leq L$ is the observation point on the beam. The resulting transfer function is meromorphic with poles occurring as

$$p_n = n^2 \pi^2 L^2 (-\zeta \pm i\sqrt{1 - \zeta^2}) \quad (3.49)$$

where $n = \pm 1, \pm 2, \dots$. The transfer function represents a stable system with uniform damping rate given by ζ and $P \in \mathcal{A}_m^\infty$.

Numerically stable evaluation of the beam frequency response can best be obtained by evaluation of the transfer function in the form

$$P(s, z) = \frac{L^2}{(\lambda_1^2 + \lambda_2^2)} \left(\frac{\sinh \lambda_2 \frac{z}{L}}{\sinh \lambda_2} - \frac{\sin \lambda_1 \frac{z}{L}}{\sin \lambda_1} \right), \quad (3.50)$$

which separates the exponential terms from the cyclic terms with respect to multiplication. In this form wide band frequency response data can be obtained with sufficient numerical precision.

The control design problem we examined is defined by a choice of the output point for regulation, $\frac{z}{L} = 0.7$, the length of the beam $L = 10.$, and the effective damping ratio, $\zeta = 0.01$. We note that since P is pseudo-meromorphic and stable the coprime factorization step is unnecessary. We take

$$N_r = N_\ell = P, \quad D_r = D_\ell = 1.$$

The resulting frequency response data for the *plant* model is shown in Figure 3.9. Clearly, the frequency response is irrational and no obvious rational approximation is evident.

The exogenous inputs describing the control problem are given as follows: the output (load) disturbance is assumed constant and has PSD given by $G_d(s) = \frac{1}{s^2}$, the feedback sensor has negligible dynamics (i.e., $F_o = F = 1$) but is subject to noise measurements characterized by PSD

$$G_{n_f}(s) = \frac{-s^2}{s^4 + 2\omega^2(1 - 2\zeta^2)s^2 + \omega^4}.$$

The control problem considered is output regulation of the beam displacement at the specified location and we therefore characterize the PSD of the set point as $G_u(s) = 0$. The PSD's for the exogenous inputs are shown in Figure 3.10.

Control design proceeds by evaluation of the tradeoff between optimal tracking cost subject to a constraint on the saturation of some critical input to the plant. Here we take $Q = 1$ so that saturation cost component is computed with respect the beam control torque. The effective optimal cost, $J = J_t + kJ_s$, tradeoff is displayed as a curve of tracking cost J_t vs. saturation cost J_s in Figure 3.13. The cost components is estimated from the sampled frequency response data by numerical approximation of (2.57)–(2.58) using

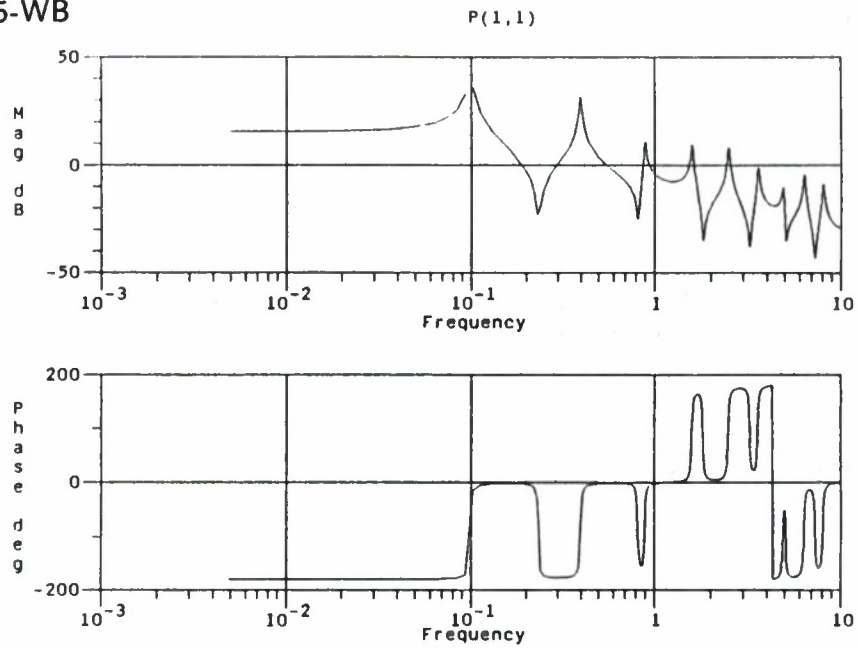


Figure 3.9: Frequency response for pinned-pinned beam control.

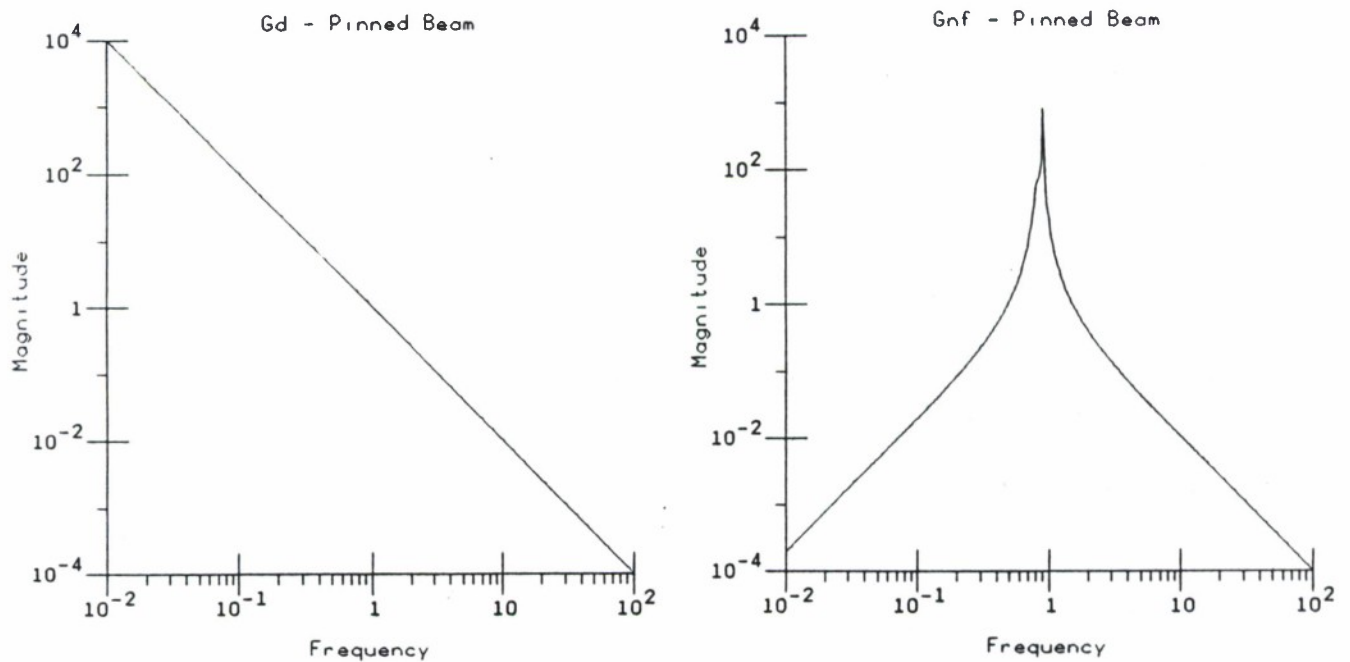


Figure 3.10: PSD for disturbance and sensor noise inputs for beam control.

rectangular quadrature. The sampled data was computed using 1024 uniform sampling of the frequency response with bandwidth $\omega_{BW} = 10$. The performance of the spectral factorization steps is displayed in Figure 3.11. The algorithm convergence is displayed by examining the size of the residual. The frequency sampled spectral factors $\Omega(s)$ for the filtering problem and $\Lambda(s)$ for the control problem are displayed in Figure 3.12.

To check the sensitivity of the computations to the choice of bandwidth we recomputed the optimal control tradeoff study using 1024 point sampling for a bandwidth of 100. The beam frequency response is shown in Figure 3.14. The tracking vs. saturation cost tradeoff for this bandwidth is displayed in Figure 3.15.

The tradeoff in control system performance for the choice of tracking vs. saturation weighting can also be displayed directly in the frequency domain by displaying the magnitude of the sensitivity function $S(s)$ and its complement $1 - S(s)$. Figure 3.16 displays these functions for several choices of the parameter k . For SISO problems, the traditional notions of gain and phase margin can be readily obtained from a Nyquist plot of the loop transmission, $P(j\omega)C(j\omega)$ which is shown for the 1024 point sampling for a bandwidth of 100 in Figure 3.17.

Once the tradeoff analysis of saturation vs. tracking is resolved the optimal controller is specified in terms of its frequency response. The choice of $k = 0.1$ achieves a saturation cost for this problem of $J_s = 7$ representing the total energy in the actuating torque signal. The resulting controller frequency response is shown in Figure 3.18 for 1024 point sampling of over a bandwidth of 100.

All frequency response plots are obtained as hardcopy from the prototype code designed for the Phase 1 effort. In a realistic design environment the frequency response data can be manipulated and displayed interactively to support tradeoff studies supporting the controller computational phase of design. In Phase 2 we propose to port this code to a dedicated workstation and to enhance the code with specific provisions for tradeoff analysis of various control law implementations.

3.4.2 Vibration Isolation for a Simple Elastic Structure.

A prototype MIMO control problem for active vibration isolation is considered with elastic dynamics of a flexible structure. To demonstrate the compatibility with available models of complex flexible structures we develop a simple finite element representation of the elastic structure response and use the resulting finite dimensional model to approximate the irrational frequency response.

The model is shown in Figure 3.19. For this simple problem we consider all motion constrained in the $x - z$ plane. The model consists of a flexible appendage attached via a one degree of freedom rotational joint to an relatively massive carriage which is supported mechanically from an inertial reference. The carriage support is modeled by a lumped stiffness and damping. The carriage is subject to a disturbance force f . Active vibration isolation is achieved in this simple model by a torque τ_b applied at the rotational joint between the flexible appendage and the carriage. Additionally, there is a torque τ_L which can be applied at the end of the appendage. Feedback control is possible using measurements of appendage angle θ and angular deformation (shear strain) $\phi(L)$ at the end of the appendage.

 RESIDUAL COMPUTATION SUMMARY

ITERATION NO.	MAX. ELEMENT	MAX. TRACE
0	0.6426E-02	0.6426E-02
1	0.1228E-04	0.1228E-04
2	0.2389E-06	0.2389E-06
EPSILON		0.1000E-05
MAXIMUM NUMBER OF ITERATIONS		11
NUMBER OF ITERATIONS TO CONVERGE ON EPSILON		2

Figure 3.11: Convergence of filter spectral factorization for pinned-pinned beam.

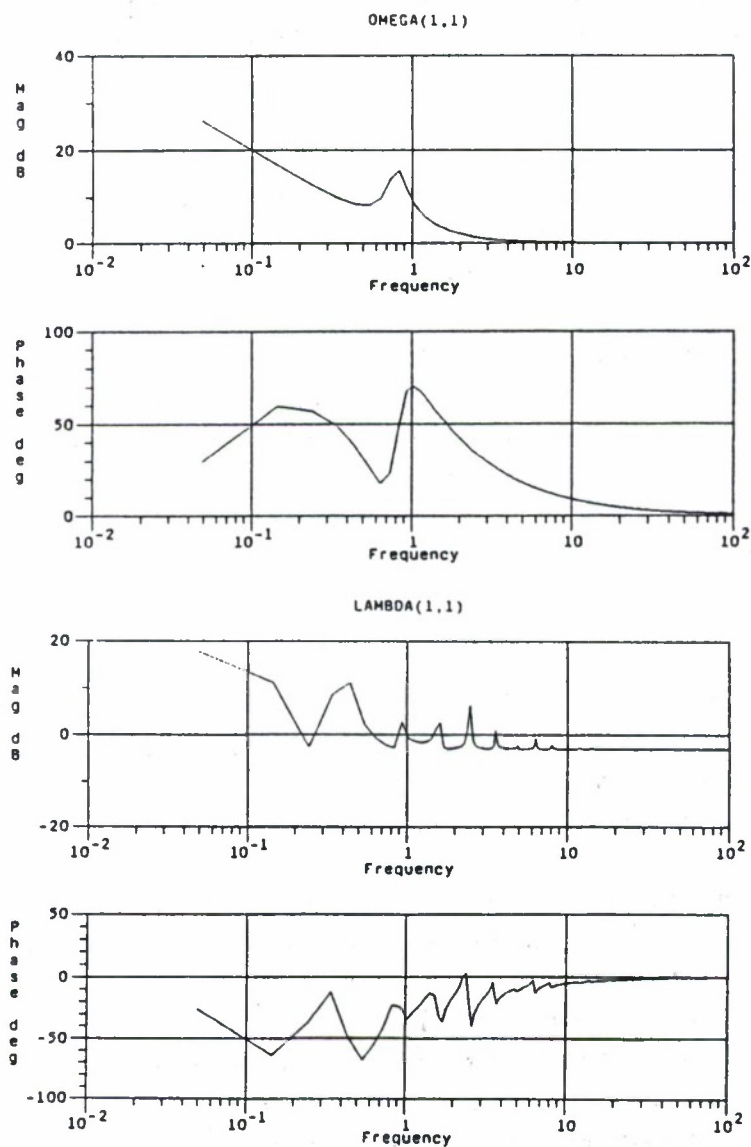


Figure 3.12: Spectral Factors for pinned-pinned beam control.

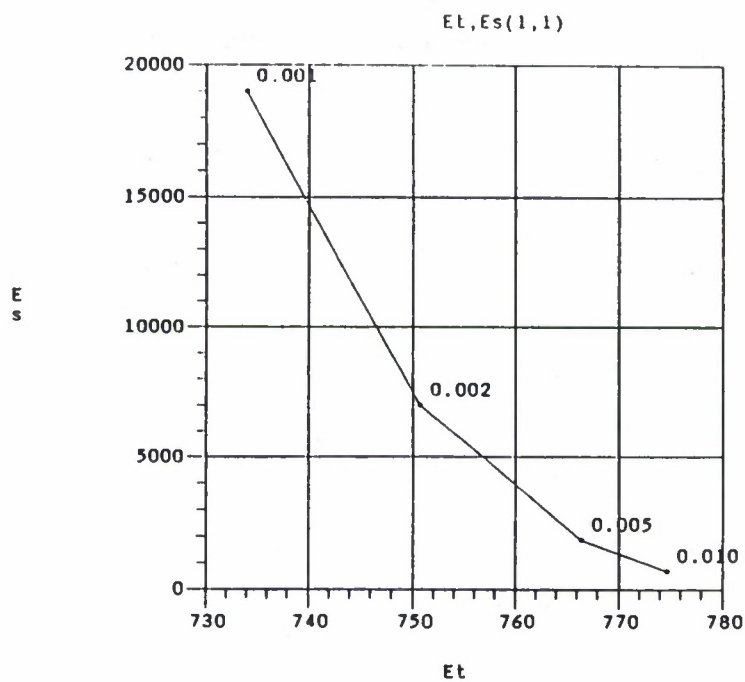


Figure 3.13: Tracking vs. Saturation Tradeoff for Beam Control.

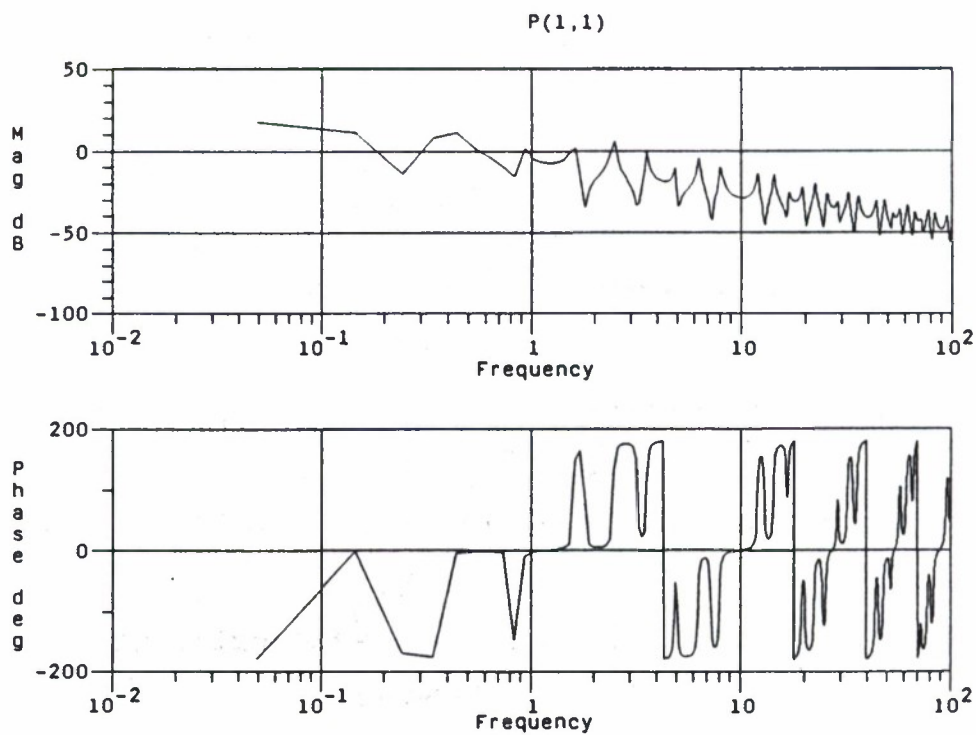


Figure 3.14: Frequency response for pinned-pinned beam control.

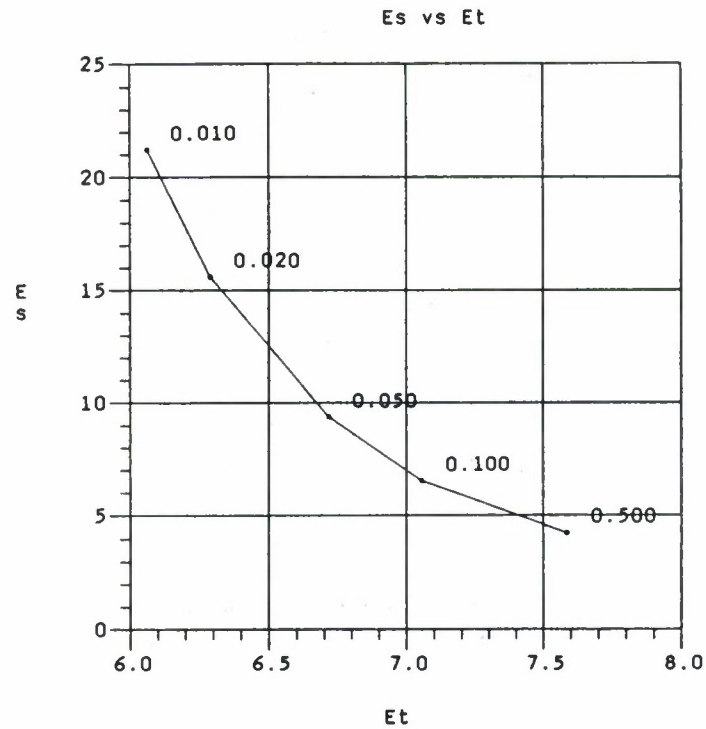


Figure 3.15: Tracking vs. Saturation Tradeoff for Beam Control.

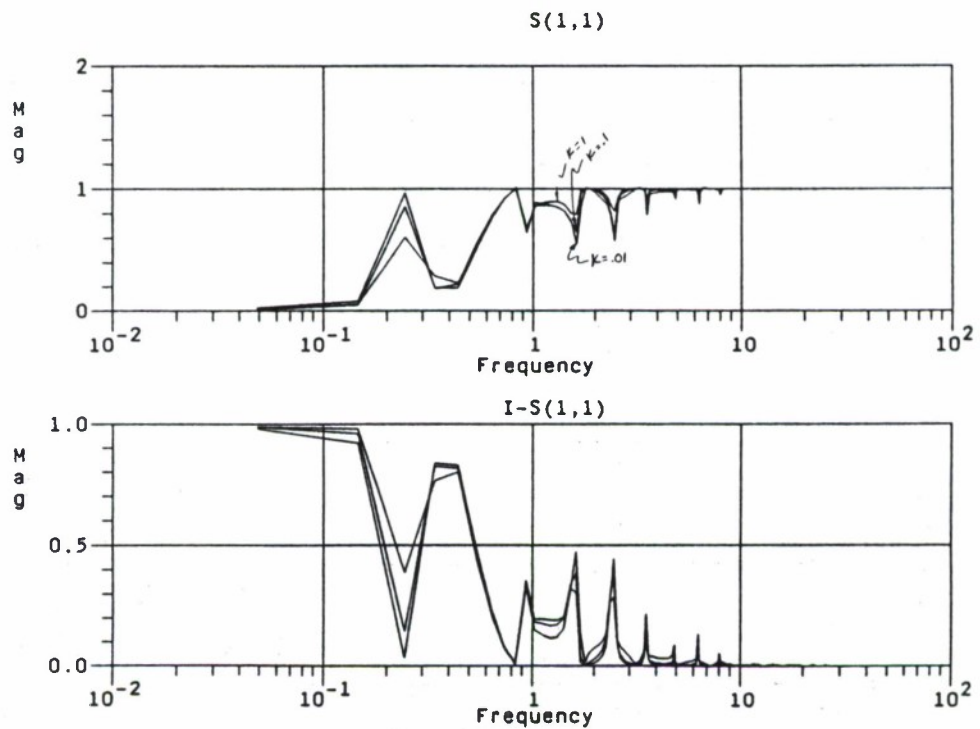


Figure 3.16: Design Tradeoff using Sensitivity Function for Beam Control.

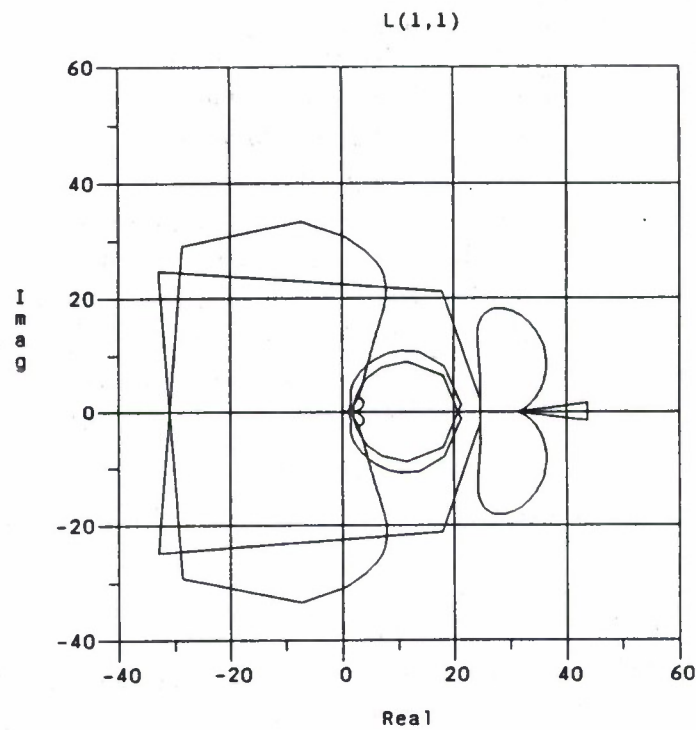


Figure 3.17: Nyquist Plot of Beam Control Loop for $k = .1$.

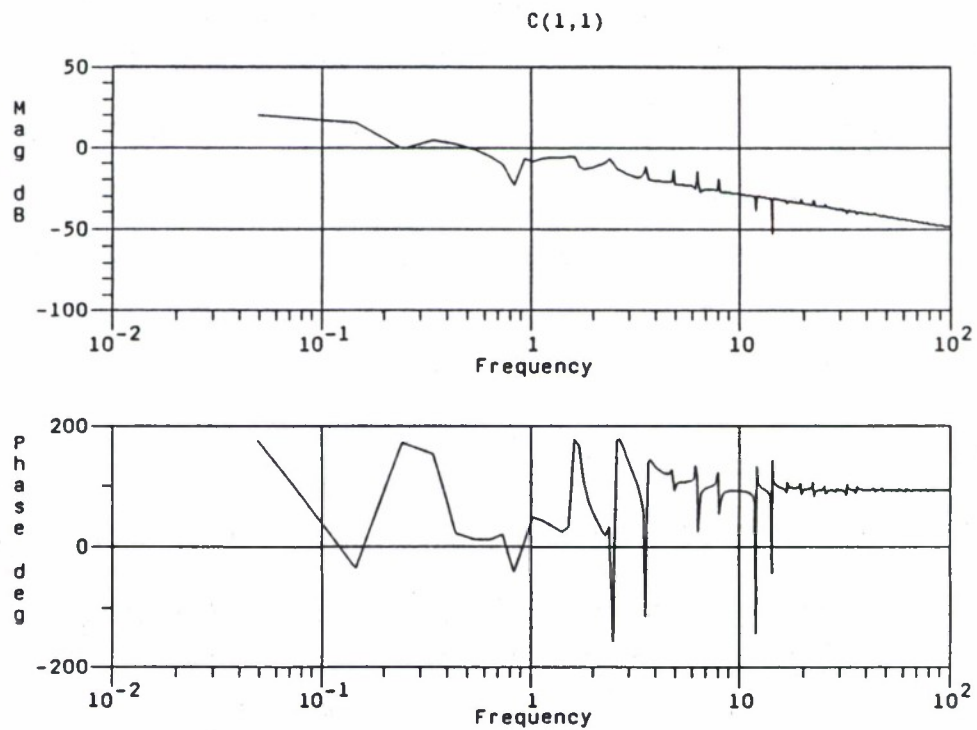


Figure 3.18: Optimal Controller Frequency Response for $k = .1$.

model parameter	value	description
m_c	0.9	mass of the carriage
k	1.0	support stiffness
b	1.0	support damping
L	15.	appendage length
ρ	0.0707	mass density of appendage
A	0.0942	area cross section for appendage
I_a	5.302	area moment of inertia for appendage
E	16.0	modulus elasticity of appendage
κG	6.4	effective shear modulus
ζ_1	0.01206	damping constants for material dissipation
ζ_2	1.697	

Table 3.3: Model Parameters for Vibration Isolation Problem.

Thus the plant transfer function $P(s)$ is 2×2 .

The dynamic model is obtained by application of Hamilton's principle in terms of the generalized coordinates $\{x, \theta, \eta(z), \phi(z)\}$ where x is the horizontal displacement of the carriage, θ is the angular displacement of the appendage at the joint, $\eta(z)$ is the lateral deformation of the appendage relative to the centerline given by θ , and $\phi(z)$ is the angular deformation of the appendage cross section over the length of the appendage; $0 \leq z \leq L$. The model parameters are given in the Table 3.3. Parameters are dimensionless and chosen to provide reasonably well scaled spectral response of typical flexible structure response.

Under the above assumptions the system kinetic energy takes the form,

$$T(\dot{x}, \dot{\theta}, \dot{\eta}, \dot{\phi}) = \frac{1}{2} m_c \dot{x}^2 + \frac{1}{2} \int_0^L \{ \rho A (\dot{x} + \dot{\eta}(z) - z \dot{\theta})^2 + \rho I_a (\dot{\theta} + \dot{\phi}(z))^2 \} dz, \quad (3.51)$$

and the system potential energy is,

$$V(x, \theta, \eta, \phi) = \frac{1}{2} k x^2 + \frac{1}{2} \int_0^L \left\{ E I_a \left(\frac{\partial \phi}{\partial z} \right)^2 + \kappa G A \left(\frac{\partial \eta}{\partial z} - \phi \right)^2 \right\} dz. \quad (3.52)$$

We also assume a dissipation function of the form,

$$R = \frac{1}{2} \int_0^L \left\{ \zeta_2 \left(\frac{\partial \dot{\phi}}{\partial z} \right)^2 + \zeta_1 \left(\frac{\partial \dot{\eta}}{\partial z} - \dot{\phi} \right)^2 \right\} dz \quad (3.53)$$

which models material losses which are expected to be dominant in terms of dissipation for space applications.

A finite dimensional model can be obtained by the Finite Element Method (FEM) by introducing, for example, assumed modes and expansions of the form,

$$\eta(t, z) \approx \Phi^T(z) \bar{\eta}(t), \quad \phi(t, z) \approx \Phi^T(z) \bar{\phi}(t),$$

where $\bar{\eta}, \bar{\phi}$ are N -vectors of FEM degrees of freedom. We prefer the introduction of "assumed modes" from FEM using collocation by splines. We note that under the above assumptions 1st order (linear) splines are sufficient [28].

Applying the above FEM approximation to the energy functions and solving the Euler-Lagrange equations for the reduced system Lagrangian $L = T - V$ obtains the dynamic equations in the form,

$$M\ddot{w}(t) + B\dot{w}(t) + Kw(t) = Eu(t), \quad (3.54)$$

$$y(t) = C_1 w(t) + C_2 \dot{w}(t),$$

where $w = [x, \theta, \bar{\eta}, \bar{\phi}]^T$, $u = [\tau_b, \tau_L, f]^T$, and $y = [\theta, \phi(L)]^T$. (Model data in this form are typically obtained from a variety of standard FEM codes such as NASTRAN.) The matrix parameters have the form

$$M = \begin{bmatrix} M_{tot} & -N_{\theta x} & N_{\eta x}^T & 0 \\ -N_{\theta x} & J_\theta & -N_{\theta \eta}^T & N_{\theta \phi}^T \\ N_{\eta x} & -N_{\theta \eta} & N_\eta & 0 \\ 0 & N_{\theta \phi} & 0 & N_\phi \end{bmatrix}, \quad (3.55)$$

$$B = \begin{bmatrix} b & 0 & 0 & 0 \\ 0 & 0 & 0 & 0 \\ 0 & 0 & B_\eta & B_{\eta \phi} \\ 0 & 0 & B_{\eta \phi}^T & B_\phi \end{bmatrix}, \quad (3.56)$$

$$K = \begin{bmatrix} k & 0 & 0 & 0 \\ 0 & 0 & 0 & 0 \\ 0 & 0 & K_\eta & K_{\eta \phi} \\ 0 & 0 & K_{\eta \phi}^T & K_\phi \end{bmatrix}. \quad (3.57)$$

Here M_{tot} is the system total mass, and J_θ is the effective rigid inertial moment for the θ motion. The other model parameters arise from the FEM approximation and are characterized by, for example, scalar expressions of the form

$$N_{\theta x} = \int_0^L \rho A z \, dz,$$

row matrices of the form,

$$N_{\eta x}^T = \int_0^L \rho A \Phi^T(z) \, dz,$$

and tridiagonal matrices of the form,

$$\begin{aligned} N_\eta &= \int_0^L \rho A \Phi(z) \Phi^T(z) \, dz, \\ K_\eta &= \int_0^L \kappa G \frac{\partial \Phi}{\partial z} \frac{\partial \Phi^T}{\partial z} \, dz \\ &\vdots \end{aligned}$$

(cf [28] for details on the development of FEM models by collocation by splines.) The matrix E is $(2 + 2N) \times 3$ with $E(1,1) = 1$, $E(2,3) = 1$, and $E(2 + 2N, 2) = 1$. The composite matrix $[C_1, C_2]$ is the transpose of the first two columns of E .

The parameters of the model were chosen to provide a spectrum for the numerical computations of the frequency response characteristic of flexible space structures with damping arising primarily from material losses and to illustrate opportunities for tradeoff in the computation of stable coprime factorization. We have also structured the control problem by choosing collocated sensing and actuation. Figure 3.20 illustrates the position of the poles and transmission zeros for the 2×2 transfer function $P(s)$ which takes inputs $(\tau_b, \tau_L)^T$ to outputs y . The effect of the disturbance loading is given by the transfer function $P_o(s)$ from f to y .

We note that the system model is unstable with one real pole in the right half plane. The unstable mode is associated with the unstable reaction of the flexible appendage which is attached to the carriage by a one degree of freedom rotational joint with no dynamic restraint. It will be required to obtain a stable coprime factorization for the system transfer function before proceeding with the numerical frequency sampling computations of the controller frequency response.

Stable coprime factorization can be directly obtained from the model (3.54), or equivalently, by transforming the model to state space form,

$$\begin{aligned}\dot{x} &= Ax + \tilde{B}u, \\ y &= \tilde{C}x,\end{aligned}\tag{3.58}$$

with

$$\begin{aligned}A &= \begin{bmatrix} 0 & I \\ -M^{-1}K & -M^{-1}B \end{bmatrix}, \quad \tilde{B} = \begin{bmatrix} 0 \\ M^{-1}E \end{bmatrix}, \\ \tilde{C} &= [C_1, C_2].\end{aligned}\tag{3.59}$$

As discussed in the previous section stable coprime factorizations can be obtained from the state space realization (cf. (3.2)–(3.4)). First, find real matrices H and F so that the eigenvalues of $A_H = A + H\tilde{C}$ (resp. $A_F = A + \tilde{B}F$) are in the left half plane. Then the coprime factors can be given as,

$$[N_\ell, D_\ell](s) = [0, I_p] + \tilde{C}[sI - A_H]^{-1}[\tilde{B}, H],\tag{3.60}$$

$$\begin{bmatrix} N_r \\ D_r \end{bmatrix} = \begin{bmatrix} 0 \\ I_m \end{bmatrix} + \begin{bmatrix} \tilde{C} \\ F \end{bmatrix}[sI - A_F]^{-1}\tilde{B}.\tag{3.61}$$

The pole/zero plots for the respective factors are shown in Figure 3.21 where we have chosen the poles of the factors by translating the real part of the unstable and nearly unstable poles (including the real pole at $s = 1.73$ and the double pole at the origin) of $P(s)$ to the left. From these figures it is clear that the transmission zeros of N_ℓ (resp. D_ℓ) are the transmission zeros (resp. poles) of P . The poles of $[N_\ell, D_\ell]$ represent the stabilizing choices of the open loop poles.

The disturbance force is modeled via a narrowband PSD centered about $\omega = 1$ given by

$$G_f(s) = \frac{-s^2}{s^4 + 2(1 - 2\zeta^2)s^2 + 1}.$$

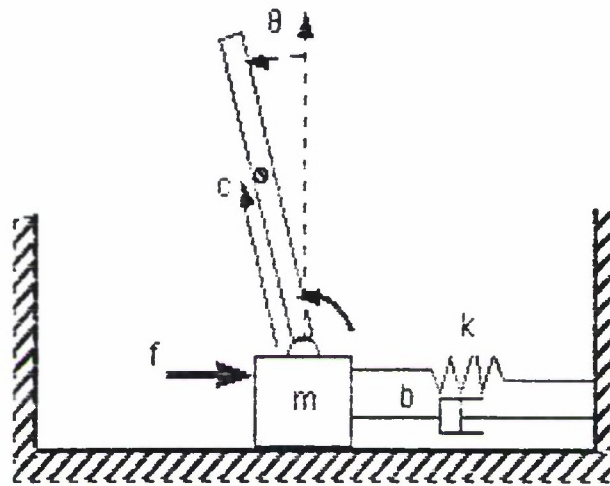


Figure 3.19: Vibration Isolation Model with Flexible Structure.

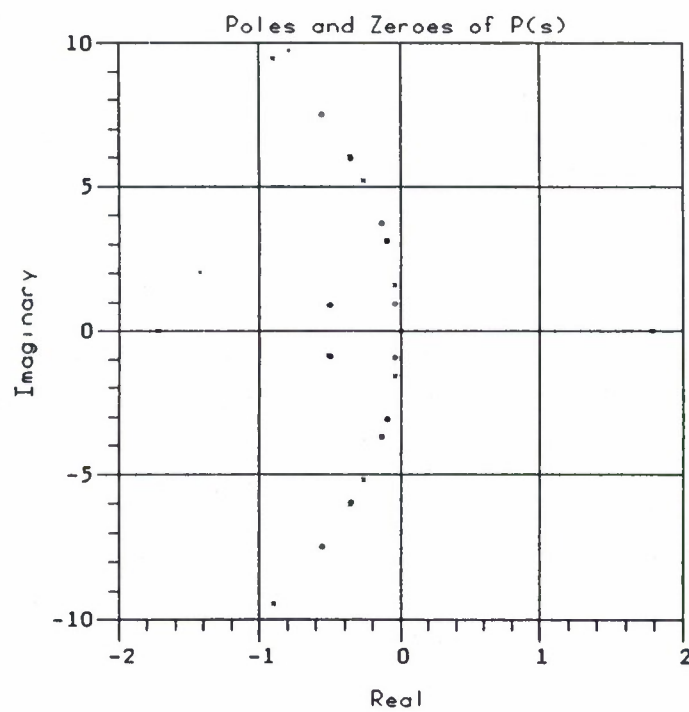


Figure 3.20: Pole/Zero plot for Vibration Isolation Model.

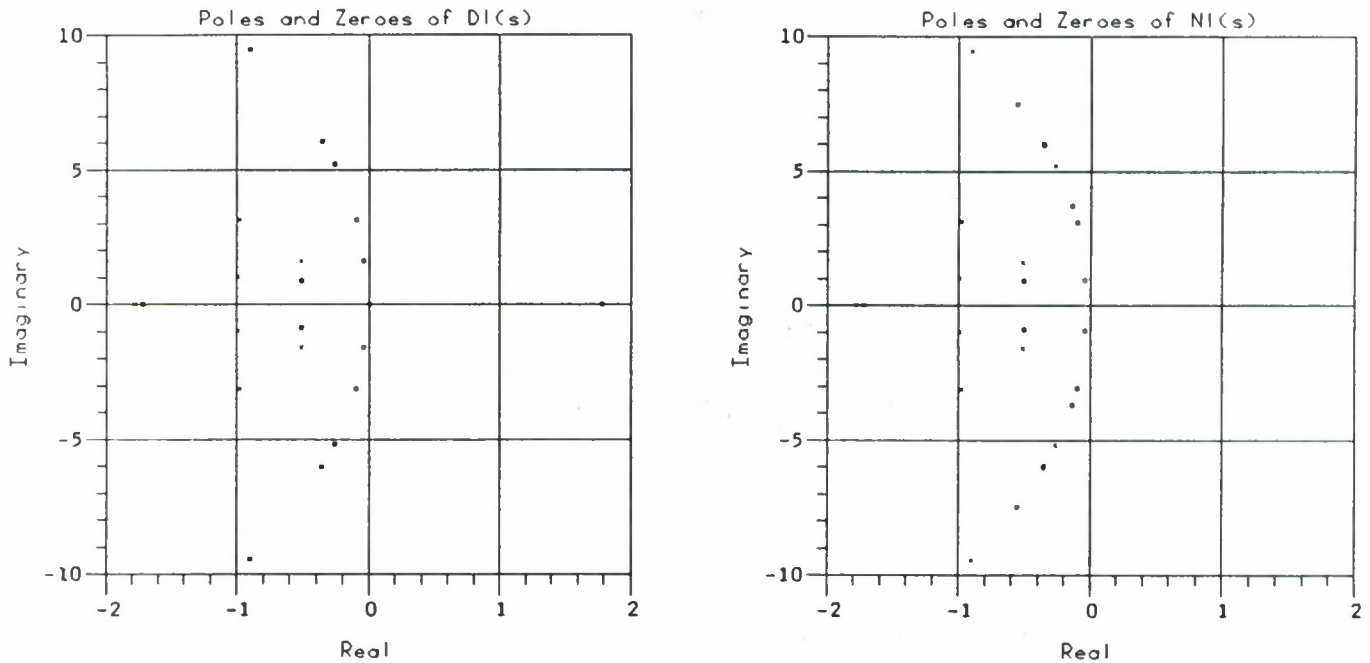


Figure 3.21: Pole/zero Locations for the Coprime Factors.

This might represent a periodic motion of some onboard subsystem components for a space craft example. Assume the displacement sensors are subject to independent, zero mean noise processes described by PSD's of the form

$$G_{n_f}(s) = \frac{-s^2}{s^4 + 2\omega^2(1 - 2\zeta^2)s^2 + \omega^4}.$$

Tradeoff analysis of tracking vs. saturation was performed and a value of $k = .5$ was chosen for the candidate design. The resulting closed loop control bandwidth can be determined from the frequency response of the 2×2 sensitivity function S and its complement $I - S$. In Figure 3.22 the singular values of these matrix frequency responses are shown plotted as dB gain vs. log frequency. From these figures one can obtain an estimate of the desired closed loop control bandwidth obtained by Wiener-Hopf optimization. Note the numerical noise evident in the singular value plots of $I - S$ for high frequencies. This is a result of the single precision computations currently implemented in the software. We display the specification of the optimal control law in terms of the computed frequency samples of its scalar components via the Bode plots in Figure 3.23.

We remark that the problem considered here is characteristic of structural vibration control problems in several ways. One important feature is evident by examination of the frequency response of the open loop plant transfer function. In Figure 3.24 we plot the minimum and maximum singular values of the frequency response of P . The rigid body mode at the origin is evident in the effective gain (i.e. maximum singular value) increasing without

bound for decreasing frequency. However, the ratio of maximum to minimum singular values is also increasing without bound for decreasing frequencies. This indicates a numerical singularity of the effective frequency response for $s = 0$. But this is characteristic of the redundant actuators and sensors for the effective rigid (i.e. low frequency) response of the appendage. It is interesting to note that even with such ill-conditioned transfer function model that the numerical algorithms for spectral factorization, causal projection, and other components of the Wiener-Hopf control design computations produce numerically stable results. We intend to direct software and algorithm development in the Phase 2 proposal toward the development of various options for extended precision computations and options for MIMO control loop shaping for transfer function models with low frequency redundancies (i.e. near singular numerical behavior).

3.5 Realtime Control Law Implementation

The frequency sampled computations obtain a *specification* for the frequency response of the ideal (optimal) controller via its sampled representation. The design engineer now has several options for implementing the control law. Typically for aerospace applications, high speed digital computers will be needed for real time control.

A general representation of the dynamic control law is in terms of a convolution,

$$u(t) = c(t) * y(t),$$

of the measurements $y(t)$ with a controller impulse response, $c(t)$. We contend that the technology for implementing high speed convolution or filtering for real time control of flexible structures is now available and can be realized using digital signal processing methods.

The convolution above can be approximated to any desired degree using a discrete time representation,

$$u(nT) = \sum_{k=0}^{k=\infty} c((n-k)T)y(nT).$$

In general such a system can be represented as a *causal recursive linear system*, i.e., one whose present output is computed from past and present inputs and outputs. However, in many cases the response can be approximated by a *nonrecursive system*; i.e., one whose present output depends only on past and present inputs. Thus a nonrecursive realization (if one exists) would take the form of a moving average,

$$u(nT) = \sum_{k=0}^m \alpha_k y((n-k)T).$$

Such a realization is often called a *Finite Impulse Response (FIR)* filter, since the effective impulse response will become zero after m time steps. If the ideal continuous controller has transfer function which is analytic in the closed right half plane and is strictly proper then its impulse response approaches zero as $t \rightarrow \infty$. Such an impulse response can be approximated arbitrarily well by a FIR filter.

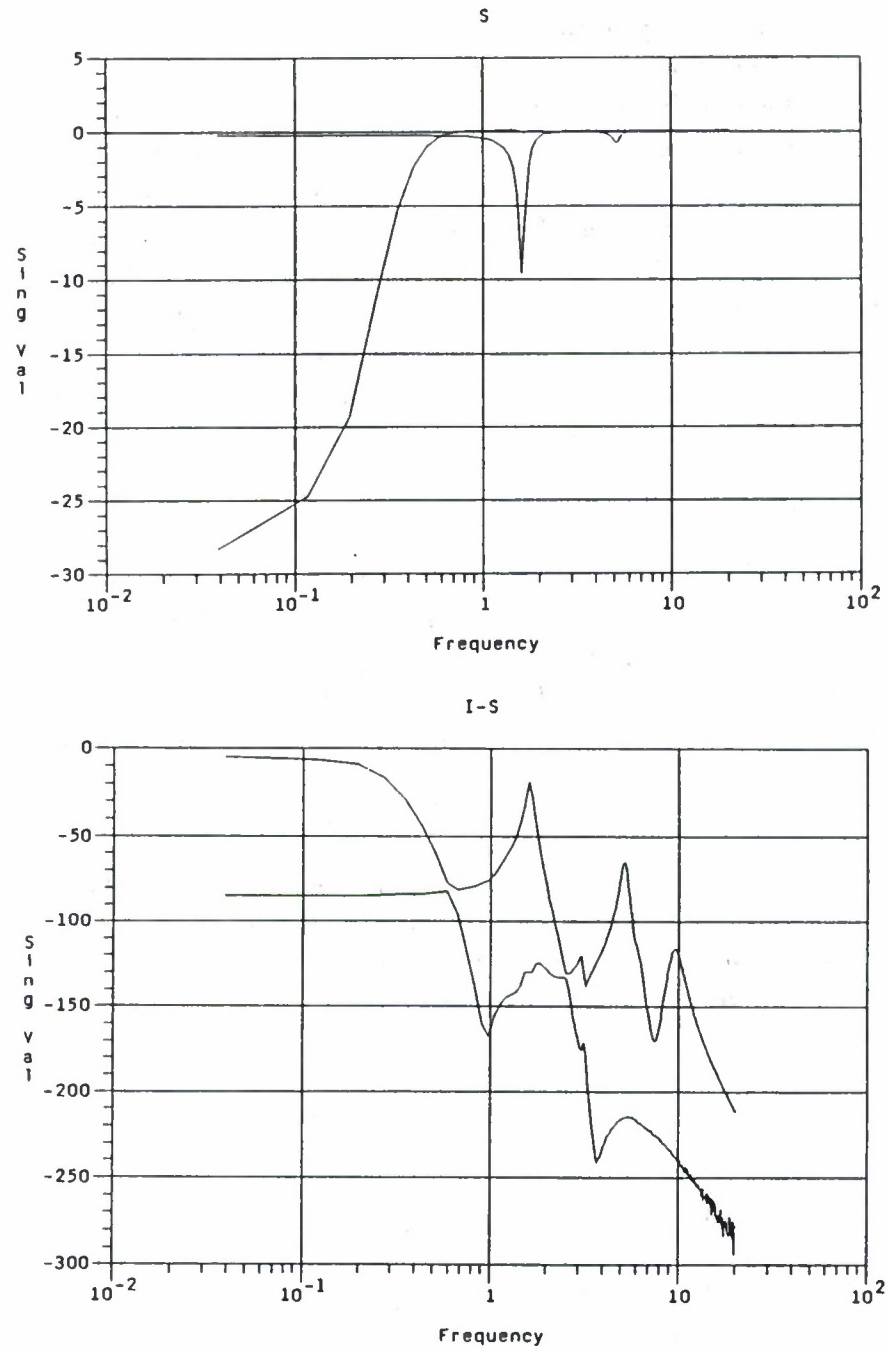
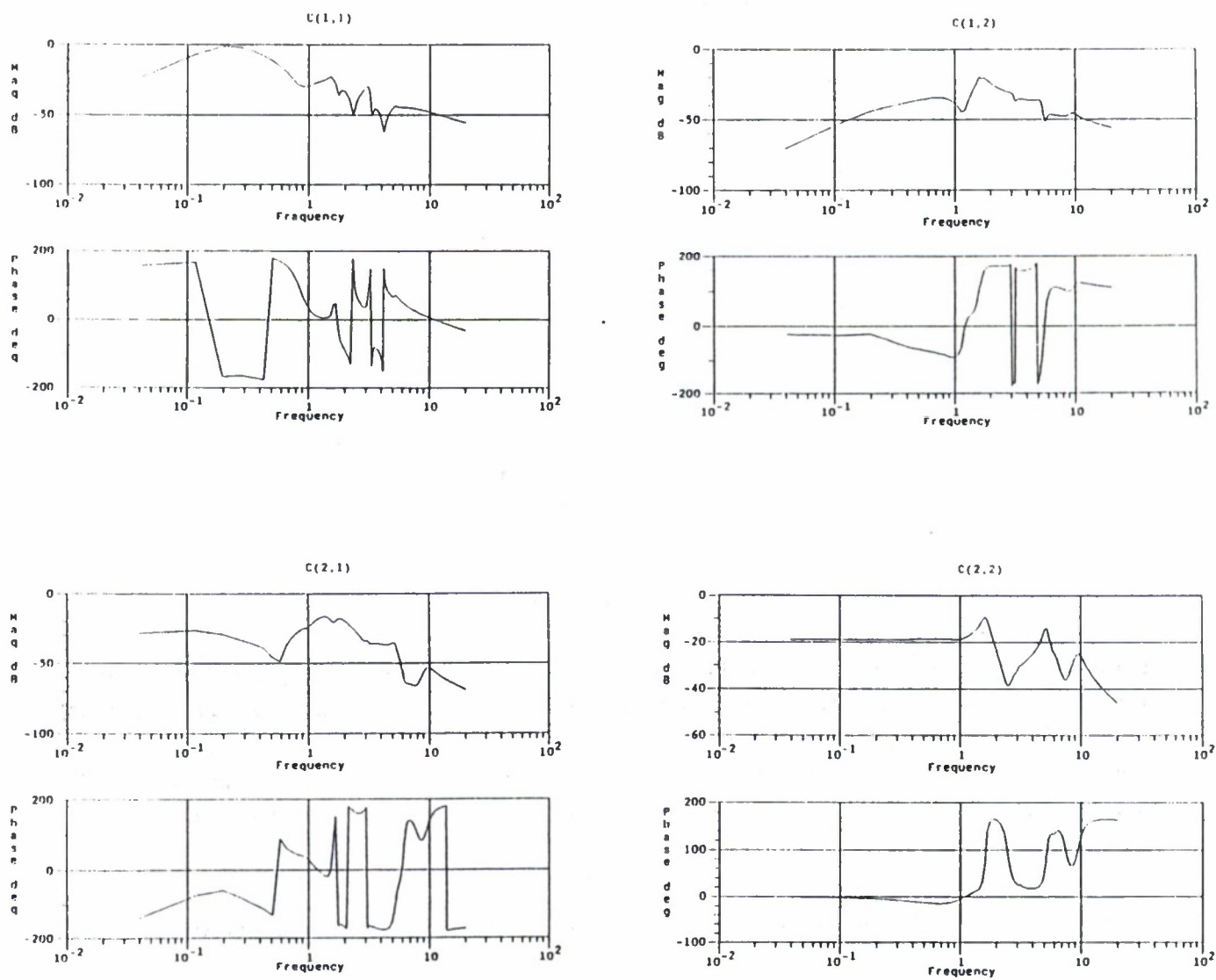
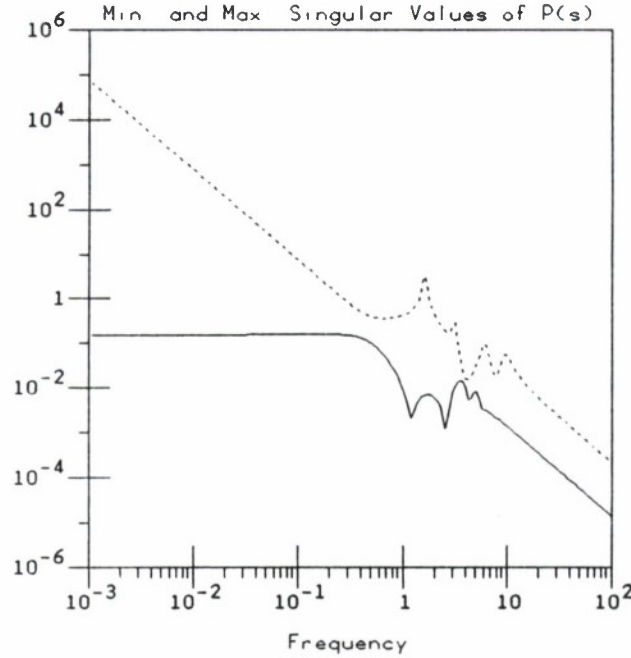


Figure 3.22: Singular Value plots of the Sensitivity Function for $k = .5$.

Figure 3.23: Bode plots for the scalar elements of $C'(s)$

Figure 3.24: Singular value plots of $P(s)$.

Frequency Sampling Filter realization. An example of an FIR filter is the *frequency sampling filter* whose frequency response is chosen to interpolate a desired frequency response by exactly matching a set of N frequency samples. Consider the case where the frequency samples are uniformly spaced. Since the filter is implemented in discrete time its transfer function can be described using z -transforms. The frequency response samples are therefore given as;

$$z_k = e^{jk2\pi/N},$$

for $k = 0, \dots, N-1$, (the N roots of unity) which correspond to the frequencies

$$\omega_k = k\omega_s/N,$$

where ω_s is the time sampling rate for the discrete time realization.

The interpolating function in the z -plane can be given as

$$F_k(z) = \frac{1 - z^{-N}}{N(1 - e^{jk2\pi/N} z^{-1})},$$

with $k = 0, \dots, N-1$. This function has the interpolating property;

$$F_k(e^{j\ell 2\pi/N}) = \begin{cases} 0 & \text{for } \ell \neq k \\ 1 & \text{for } \ell = k \end{cases}$$

If we take the desired frequency samples as C_k then the transfer function

$$G(z) = \sum_{k=0}^{N-1} C_k F_k(z)$$

will realize the frequency sampling filter. It is easy to show that the frequency sampling filter has transfer function

$$G(z) = \frac{1 - z^{-N}}{N} \sum_{k=0}^{N-1} \frac{C_k}{1 - e^{jk2\pi/N} z^{-1}} = \sum_{\ell=0}^{N-1} c_{\ell} z^{-\ell}$$

where the coefficients are given as

$$c_{\ell} = \frac{1}{N} \sum_{k=0}^{N-1} C_k e^{j(2\pi/N)\ell k}$$

for $\ell = 0, \dots, N - 1$.

The coefficients c_0, \dots, c_{N-1} are known as the *Inverse Discrete Fourier Transform (IDFT)* of the sequence C_0, \dots, C_{N-1} . Thus a simple implementation of the frequency sampling filter which has been used in a wide range of digital signal processing applications is described as follows. Sample the input time waveform $y(t)$ with uniform sampling rate and sequentially load the samples in a buffer. After every $k < N$ samples are stored in the input buffer the convolution is implemented by performing a DFT of the input sequence. Then perform IDFT of the product of this result with the frequency samples (i.e., the coefficients C_k) to obtain the sampled time representation of the output $y(t)$. The output buffer is then sequentially clocked to the output D/A channel. This illustrates that the delay in processing is dependent on the computational delay for DFT processing of N length sequences. It is well known that the convolution operation just described is most efficiently implemented using the *Fast Fourier Transform (FFT)*—a special form of the DFT optimized for minimum number of multiplications [26].

In general, the problem of realizing closed loop controller by FIR filters is complicated by the available processing speeds and the duration of the ideal continuous time controller impulse response. The construction of stabilizing controllers via stable coprime factorization can potentially play a significant role in practical aspects of FIR-based controller realization.

Consider a general stabilizing feedback controller given in terms of the relation (2.41). The control law can be expressed in the frequency domain as

$$u(s) = C(s)y(s)$$

or equivalently,

$$u(s) = [Y(s) + D_r(s)K(s)]\xi(s) \quad (3.62)$$

$$X(s)\xi(s) = y(s) + N_r(s)K(s)\xi(s), \quad (3.63)$$

where we take X, Y, N, D, K can be chosen to be “arbitrarily stable”. By this we mean that their respective poles can be chosen to be to the left of a vertical axis in the complex plane whose real part can be chosen arbitrarily far into the left half plane. The controller $C(s)$ may not be arbitrarily stable however since X^{-1} may have poles to the right of the arbitrarily chosen vertical line. Indeed, in some cases C may not be stable at all in which case implementation of the control law by direct FIR processing is not feasible. However, it is easy to show that realization can be obtained by feedback.

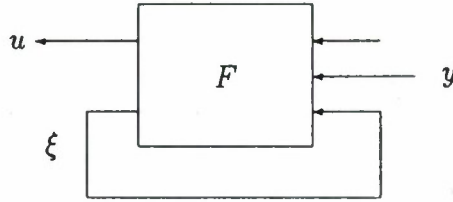


Figure 3.25: Option for Stable FIR controller implementation

To see how this can be we obtain X in the form,

$$X = U - \tilde{X}$$

where U has an “stable” inverse (i.e. has all poles to the left of the arbitrary vertical line) and \tilde{X} has only “unstable” poles. Note that for most flexible structure models \tilde{X} will be rational. Then we can write the control law in the form,

$$\begin{pmatrix} u \\ \xi \end{pmatrix} = \begin{bmatrix} 0 & [Y + D_r K] \\ U^{-1} & [U^{-1} N_r K - I] \end{bmatrix} \begin{pmatrix} y \\ \xi \end{pmatrix} = F \begin{pmatrix} y \\ \xi \end{pmatrix}$$

which can be implemented as a stable filter with external feedbacks as shown in Figure 3.25. Note that each component of this feedback realization of the control law is arbitrarily stable.

We have shown that the controller can be realized by a feedback connection of components each of which has impulse response which can be tailored for specific implementation requirements of the components available to the designer. In particular, each component is stable and can be realized by an FIR filter. In Phase 2 we will focus on implementation considerations for FIR type processing and the options for feedback realizations of this type seems to offer increased flexibility for such designs.

4 Conclusions and Directions

Results from the Phase 1 study have demonstrated that the computational problem of frequency domain design can be solved using frequency sampling. As such the computations can be readily extended to certain classes of irrational transfer functions; such as typically arise in control of flexible structures. Advantages of the approach include:

1. The computation of control by frequency response sampling can embrace design problems consisting of both irrational and rational transfer function models using the same algorithms.
2. The required frequency response data for model building can be obtained from analytical models of the elastic dynamics, finite element models of structural responses, and/or empirical data obtained from measurements on full or partial scale models.
3. The flexibility of control law implementation is left to the design engineer.

We believe that a natural approach for flexible structure control law implementation is to realize the required processing (i.e., real time convolution) by discrete time methods and to implement using advanced high speed VLSI technology. For real time control applications the processing delay incurred in FIR implementation is a critical factor which may effect the system stability margins. The major goal of the phase 2 effort will be to demonstrate that high speed implementations can reduce the processing delay to acceptable levels for application to control of flexible structures.

Another important issue in realtime implementation arises when the ideal controller $C(s)$ is open loop unstable (i.e., has poles in the closed right half plane). In such cases the impulse response can not be directly approximated by an FIR filter. However, we have shown that the impulse response can be realized by a feedback interconnection of FIR filters [18]. Moreover, the flexibility inherent in the algebraic description of all stabilizing controllers for a given plant transfer function suggests several new options for controller realization by FIR processing which we will propose to investigate further in Phase 2.

References

- [1] M. Balas, "Trends in large space structure control theory: fondest hopes, wildest dreams," *IEEE Trans. Auto. Cntrl.*, vol. AC-27, pp. 522-535, 1984.
- [2] W. Bennett and H. Kwatny, "Continuum modeling of flexible structures with application to vibration control," *AIAA J.*, January 1989. to appear.
- [3] D. Youla, H. Jabr, and J. J.J. Bongiorno, "Modern Wiener-Hopf design of optimal controllers-parts I and II," *IEEE Trans. on Auto. Cntrl.*, vol. AC-30, no. 7, pp. 3-13 and 319-338, 1976.
- [4] T. Kailath, *Linear Systems*. Prentice-Hall, 1980.
- [5] J. C. Doyle, "Robustness of multiloop linear feedback systems," in *IEEE Conf on Dec. and Control*, (San Diego, CA), pp. 12-18, 1979.
- [6] A. N. Michel and R. K. Miller, *Qualitative Analysis of Large Scale Dynamical Systems*. Academic Press, 1977.
- [7] J. Gibson, "An analysis of optimal modal regulation: convergence and stability," *SIAM J. Cntrl and Optim.*, no. 5, pp. 686-707, 1981.
- [8] D. L. Russell, "On mathematical models for the elastic beam with frequency-proportional damping," Tech. Rep., Math. Res. Cntr. Univ. of Wisconsin, 1986.
- [9] E. Zauderer, *Partial Differential Equations of Applied Mathematics*. New York: John Wiley and Sons Inc., 1983.
- [10] I. Stakgold, *Green's Functions and Boundary Value Problems*. NY: John Wiley and Sons Inc., 1979.
- [11] A. G. Butkovskiy, *Green's Functions and Transfer Functions Handbook*. Chichester, England: Ellis Harwood Ltd., 1982.
- [12] M. Vidyasagar, *Control System Synthesis: A Factorization Approach*. MIT Press, 1985.
- [13] J. Baras, "Frequency domain design of linear distributed systems," in *Proc. of 19th IEEE CDC*, Dec. 1980.
- [14] J. S. Baras, "Complex variable methods in the control of distributed systems," 1985. Presented at NSF, SIAM, AFOSR Workshop on Control of Distributed Systems.
- [15] J. S. Baras, "Complex variable methods in distributed parameter control systems," in *Frontiers of Applied Mathematics*, (H. Banks, ed.), 1987. to appear.
- [16] W. Bennett, H. Kwatny, and J. Baras, "Frequency domain design of robust controllers for large space structures," Tech. Rep. SEI TR-86-11, SEI, November 1986. Final Report, NASA Contract No. NAS1-18209.
- [17] C. Berenstein and D. Struppa, "On explicit solutions to the Bezout equation," *Systems and Control Letters*, 1985.
- [18] W. H. Bennett, "Computation and implementation of precision control for flexible structures," in *Proc. Com Con 88*, Oct. 1988.

- [19] J. Davis and R. Dickinson, "Spectral factorization by optimal gain iteration," *J. Appl. Math.*, vol. 43, pp. 389-301, 1983.
- [20] W. Bennett and I. Yan, "A computer algorithm for causal spectral factorization," in *Proc. 1988 NAECON*, May 1988.
- [21] I. Gohberg and M. Krein, "Systems of integral equations with kernel depending on the difference of the arguments," *Amer. Math. Soc. Trans.*, vol. 14, pp. 217-287, 1960.
- [22] F. Stenger, "The approximate solution of Wiener-Hopf integral equations," *J. Math. Analysis and Applic.*, vol. 37, pp. 687-724, 1979.
- [23] B. Anderson and J. Moore, *Linear Optimal Control*. Prentice Hall, Inc., 1971.
- [24] W. Bennett and H. Kwatny, "Robustness issues in control of flexible systems," in *Proc. 1987 ACC*, June 1987.
- [25] I. Digital Signal Processing Committee, ed., *Programs for Digital Signal Processing*. IEEE Press, 1979.
- [26] A. Oppenheim and R. Schafer, *Digital Signal Processing*. Englewood Cliffs, N.J.: Prentice Hall, Inc., 1975.
- [27] J.J.Dongarra, C.B.Moler, J.R.Bunch, and G.W.Stewart, *LINPACK Users' Guide*. SIAM Press, 1979.
- [28] W. H. Bennett, G. L. Blankenship, H. G. Kwatny, and O. Akhrif Tech. Rep. SEI-88-11-15-WB, SEI, November 1988. Annual Report to AFOSR/AFSC.